GEODESIC SHELLS

by

PETER RICHMOND GIRLING

B. A. Sc., UNIVERSITY OF BRITISH COLUMBIA, 1954

A THESIS SUBMITTED IN PARTIAL FULFILMENT OF

THE REQUIREMENTS FOR THE DEGREE OF

M. A. Sc.

IN THE DEPARTMENT

of

CIVIL ENGINEERING

WE ACCEPT THIS THESIS AS CONFORMING TO THE

REQUIRED STANDARDS.

THE UNIVERSITY OF BRITISH COLUMBIA

APRIL 1957

ABSTRACT

The analysis and design is presented for a shell composed of flat triangular plates approximating a smooth spherical shell. The geometry is based on the subdivision of the icosahedron and dodecahedron into many plane triangles. All corners of these triangles lie on a circumscribing sphere so that as the triangles become more numerous, the shell more nearly approximates a true sphere. The geometry is tabulated for a few of the possible subdivisions but may have to be carried further if a particularly large shell composed of relating small triangles is required. While some of the geometry is similar to geodesic domes already constructed, the structural analysis is entirely different. Previous geodesic domes are space trusses where the applied loads are supported predominantly by axial force in the truss bars. The structures considered here are frameless and the loads are therefore supported by shell action. The exact analysis to such a shell was not obtained since the solution is not composed of tabulated functions. However, an approximate analysis is presented which, in part, is a modification of smooth shell theory. Since the shell is composed of flat plates, the bending and buckling of individual triangles are additional design problems considered that are not present in more conventional shell design.

In order to verify parts of the theoretical analysis, experimental studies were conducted with a plexiglas model. The experimental results verify the application of smooth shell theory to geodesic shells and determine the distribution of membrane stress. Finally the various design aspects are brought together and illustrated by the inclusion of the design notes for a typical shell.

In presenting this thesis in partial fulfilment of the requirements for an advanced degree at the University of British Columbia, I agree that the Library shall make it freely available for reference and study. I further agree that permission for extensive copying of this thesis for scholarly purposes may be granted by the Head of my Department or by his representative. It is understood that copying or publication of this thesis for financial gain shall not be allowed without my written permission.

Department of Civil Engineering

The University of British Columbia,
Vancouver 8, Canada.

Date April 15, 1957

ACKNOWLEDGEMENT

The writer wishes to express appreciation to the Plywood Manufacturers Association of British Columbia for financial assistance in the preparation of this thesis. He also expresses his thanks to his supervisor, Dr. R. F. Hooley, who donated much of his time not only to the formulation of the basic ideas but also to the guiding of the project to a conclusion with help and encouragement. He also expresses his appreciation to Dr. D. Moore of the Department of Electrical Engineering for his help and interest in the experimental work.

CONTENTS

GRAPHS

NOTATIONS

ρ, φ, θ	Spherical co-ordinates
r_1, r_2	Radii of curvature of a shell
N_φ, N_θ, $N_{\varphi\theta}$	Membrane forces per unit length in a shell
x,y,z	Rectangular co-ordinates
w	Deflection in the z direction
Nn,Nt,Nnt	Normal and shearing forces per unit length of plate
Mn,Mt,Mnt	Bending and twisting moments per unit length of plate
Qn,Qt	Shearing force per unit length of plate
σ	Normal stress component
τ	Shearing Stress component
ϵ	Normal Strain
γ	Shear strain
E	Modulus of Elasticity
μ	Poisson's ratio
D	Flexural rigidity of a plate
h	Thickness of a plate or shell
p	Intensity of load on a shell
q	Intensity of a uniformly distributed load on a plate
X,Y,Z	Components of load in the x, y, z directions respectively
R	Resultant load on a section of shell
a	Altitude of an equilateral triangle
δ	Grid or net interval
I	Moment of inertia
Z	Section modulus

CHAPTER I

A. INTRODUCTION

A thin shell curved in two directions is an exceptionally strong and light weight structural element. A ping pong ball, an egg shell, a car roof and a balloon are only a few examples of doubly curved shells. Considering the behaviour of an egg shell, we realize that it is capable of withstanding tremendous compressive forces. Failure is caused by a concentrated load over a relatively small area or by impact.

The characteristic of high strength is due to two factors. First, the doubly curved surface has a high resistance to buckling. Second, the loads are carried almost entirely by forces in the plane of the shell or membrane forces. The significance of the second factor is that there is little bending moment in the shell under ideal conditions. This can be illustrated by considering one of the examples previously mentioned, a balloon. A rubber membrane, regardless of any applied tensile stress, has no bending resistance. Therefore, all loads applied to an inflated balloon can only be carried by membrane stress or, in this case, a reduction of the tensile stress. Thus symmetrical or unsymmetrical loads are supported by membrane action alone.

This characteristic may also be explained mathematically if we compare an arch and a shell. Stresses in an arch are governed by an ordinary differential equation to which there is only one form of solution. The solution is represented by the equilibrium polygon or thrust line. When the equilibrium polygon and the arch axis coincide, there is only direct stress in the arch. However, when two do not coincide, there is bending as well as direct stress. It is evident then that direct stress without bending is obtained only by one form of loading since the ordinary differential equation has but one form of solution. On the other hand, stresses in a shell are governed by a partial differential equation to which there are an infinite number of forms of solution. The solution in this case is represented by an equilibrium surface rather than by an equilibrium polygon. The solution chosen is that one where the equilibrium surface coincides with the shell. Thus under every continuous loading the form of solution gives only direct or membrane stresses. Discontinuous loads are excepted since solutions to the partial differential equations can also be discontinuous whereas the shell may not be.

There are, however, ways by which bending can occur in a shell. Under any given loading the membrane forces cause certain deformations of the shell. The deformations cause a small change of radius of the shell ΔR where R is measured to the inside surface of the shell. The strain on the inside of the shell is

$$\frac{\Delta R}{R}$$

and on the outside is

$$\frac{\Delta R}{R + t}$$

Where t is the thickness of the shell. However $t \ll R$ for thin shells so that practically speaking the strain is uniform across the thickness and the moment is therefore zero.

From a practical point of view, it is necessary to support the shell on a ring girder. This procedure produces bending stresses in the shell in the immediate vicinity of the ring support. The strains in the shell due to the membrane forces produce deformations causing a horizontal deflection of the shell. The forces exerted by the shell on the ring girder also produce deformations of the ring girder. Since the deformations of the shell must be the same as those in the ring girder extra forces are induced. These are a horizontal force and a moment. The resultant moment is of a local nature and dies out exponentially in a distance of ten to twenty times the shell thickness.

Finally a concentrated load also produces bending stresses in the immediate vicinity of the load. The resulting moment is similar to that produced by a ring support and dies out exponentially in about the same distance. Where bending stresses are produced, the shell may sometimes be strengthened by increasing the thickness and adding re-inforcing.

The design of a shell is commenced by determining the membrane stresses assuming the bending stresses to be zero. Since unsymmetrical loads produce only membrane stress, the maximum stress is obtained where dead load plus live load act on the whole shell. The local bending stresses are then superimposed on the membrane stresses.

Before proceeding further, it is necessary to consider in more detail a shell of revolution. The surface of such a shell is obtained by revolving a plane curve about some axis in the plane of the curve. There are, however, critical shapes that should be avoided. As a general rule, the radii of curvature should be of the same order of magnitude as the span or maximum diameter of the shell. Very shallow shells have high membrane forces. Going to the limit, if the shell is flat for any finite distance, the loads are no longer supported by membrane forces but by shears and bending moments.[1]

The following sections give the equations for symmetrical and unsymmetrical loads and tabulate the solution for a few specific cases. These solutions will be required later when considering the geodesic shell.

B. SHELL OF REVOLUTION - SYMMETRICAL LOAD.

An element of area is cut from the shell by two meridians and two parallel circles as shown in Fig. 1 - 1. The radii of curvature at a point are defined as r_1 in the meridian plane and r_2 in the plane perpendicular to the meridian. The radius of the parallel circle, denoted by r, is then equal to $r_2 \sin\varphi$ and the area of the element is $r_1 \; r_2 \sin\varphi \, d\varphi \, d\theta$.

1 An example of this is the curve $y = K\,(ax)^n$. If n is large then that part for a $x < 1$ is very flat.

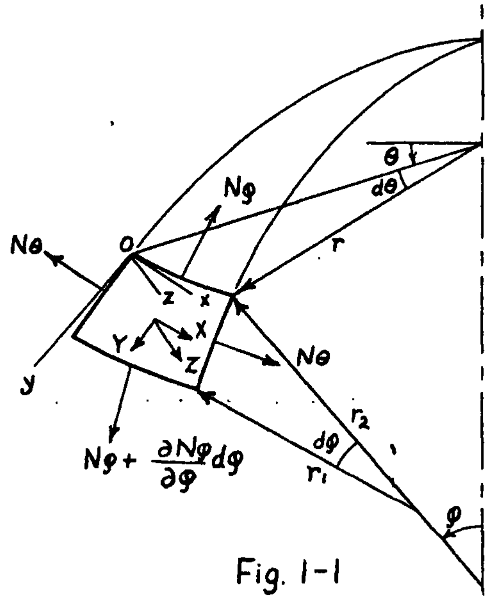

Fig. 1-1

For a symmetrical load, only normal forces act on the element since shear forces would produce unsymmetrical deformations. $N\varphi$ and $N\theta$ denote the normal forces per unit arc length. From symmetry, it can also be concluded that $N\theta$ does not vary with θ and is therefore the same on either side of the element. The external load per unit area of shell in this case acts in the meridian plane and can be resolved into two components, Y and Z, tangent and perpendicular to the element respectively.

Three equations of equilibrium of the element may be written by equating to zero the sum of the forces in the X, Y and Z directions. However, one of these equations, the sum of the forces in the X direction is automatically satisfied by symmetry. There remain two equations with two unknowns and the structure is therefore statically determinate.

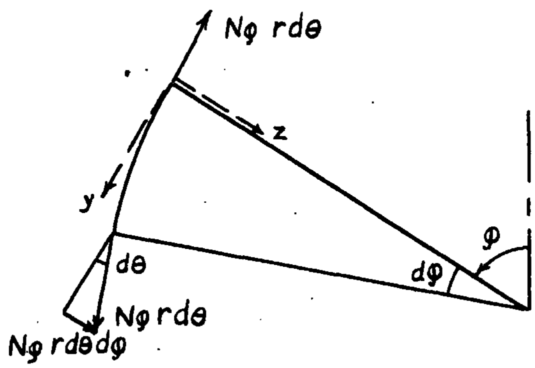

The force on the top and bottom of the element is $N_\varphi\, r\, d\theta$ and $(N_\varphi + dN_\varphi)(r + dr)\, d\theta$ respectively. Neglecting the terms of higher order, these forces have a component in the z direction of $N_\varphi\, r\, d\theta\, d\varphi$ (Fig. 1 - 2) Referring to Fig. 1 - 3 shows that the horizontal force $N_\theta\, r_1\, d\varphi$ on the sides of the element have a component $N_\theta\, r_1\, d\varphi\, d\theta$ in the direction of the radius of the parallel circle. From Fig. 1 - 4, the component in the z direction is $N_\theta\, r_1\, d\varphi\, d\theta \sin\varphi$. Equating to zero the sum of the forces in the z direction

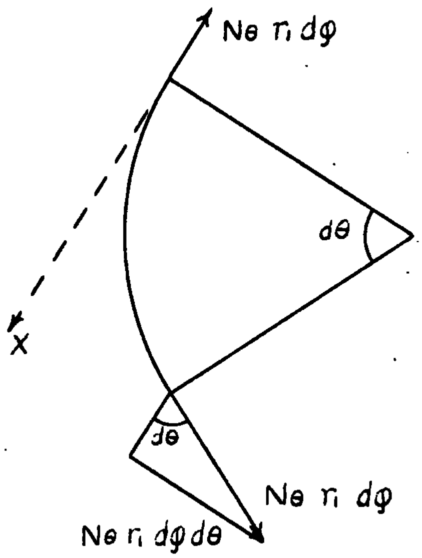

Fig 1 - 3

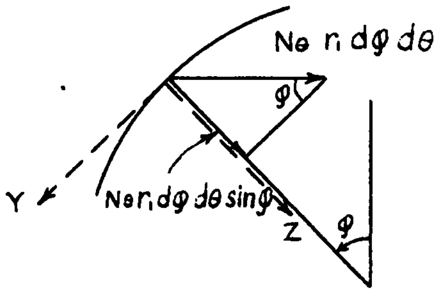

Fig 1 - 4

gives

$$N_\varphi\, r\, d\varphi\, d\theta + N_\theta\, r_1 \sin\varphi\, d\varphi\, d\theta + Z\, r\, r_1\, d\varphi\, d\theta = 0$$

Cancelling $d\varphi\, d\theta$ and dividing through by $r\, r_1$, the equation reduces to

$$\frac{N_\varphi}{r_1} + \frac{N_\theta}{r_2} = -Z \qquad (1-1)$$

A similar procedure carried out for the forces in the Y direction yields a differential equation in $N\varphi$ and $N\theta$. The solution of a differential equation is avoided, however, by considering the equilibrium of the portion of the shell above a parallel circle instead of the equilibrium of the element. Equating to zero the sum of the vertical forces, with reference to Figure 1 - 5, the equilibrium equation is

$$N\varphi \sin\varphi \cdot 2\pi r + R = 0 \qquad (1-2)$$

where R is the resultant load on the section of shell considered.

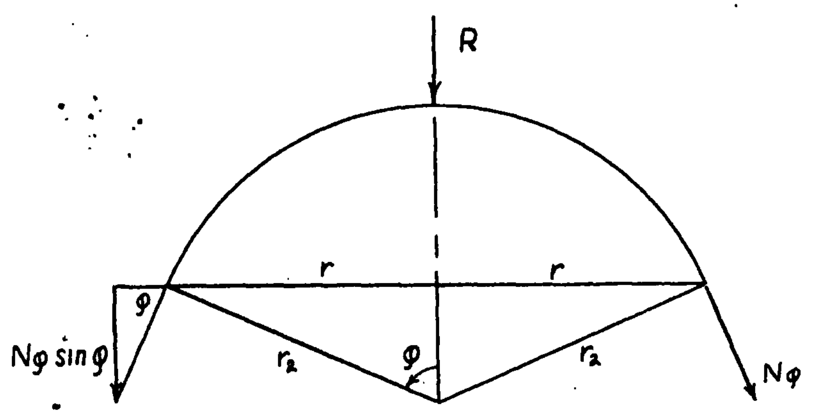

FIG. 1 - 5

The solution of the membrane forces for a given loading requires first the direct solution of Equation 1 - 2 for $N\varphi$. This value is then substituted in Equation 1 - 1 and solved for $N\theta$. The use of these equations is illustrated by considering a few special cases in the following subsections.

1 SPHERICAL SHELL OF CONSTANT THICKNESS UNDER DEAD LOAD

In a spherical shell, $r_1 = r_2 = \rho$ and $r = \rho \sin\varphi$. The surface area of a shell above the parallel circle defined by φ_1, is

$$\int_{\varphi=0}^{\varphi=\varphi_1} 2\pi r r_2 \, d\varphi = 2\pi\rho^2 \int_{\varphi=0}^{\varphi'=\varphi_1} \sin\varphi \, d\varphi \qquad (1-3)$$

Since the load on the shell is constant per unit of shell area and equal to p, then the total load on the shell is

$$R = 2\pi\rho^2 p \int_0^{\varphi} \sin\varphi \, d\varphi = 2\pi p\rho^2 (1 - \cos\varphi) \qquad (1-4)$$

Equation (1 - 2) then gives

$$N\varphi = - \frac{p\rho(1-\cos\varphi)}{\sin^2\varphi} = - \frac{p\rho}{1+\cos\varphi} \qquad (1-5)$$

Noting that the Z component of the load is $p\cos\varphi$, Equation (1 - 1) gives

$$N\theta = -p\rho \left[\cos\varphi - \frac{1}{1+\cos\varphi} \right] \qquad (1-6)$$

Equations (1 - 5) and (1 - 6) are plotted in Graph 1 - 1. The Graph show that $N\varphi$ is always compressive, increasing to a maximum compressive force at $\varphi = 90°$. On the other hand, $N\theta$ is compressive for small values of φ but turns to tension at $\varphi = 51°50'$.

Membrane Forces in a Spherical Shell of Constant Thickness.

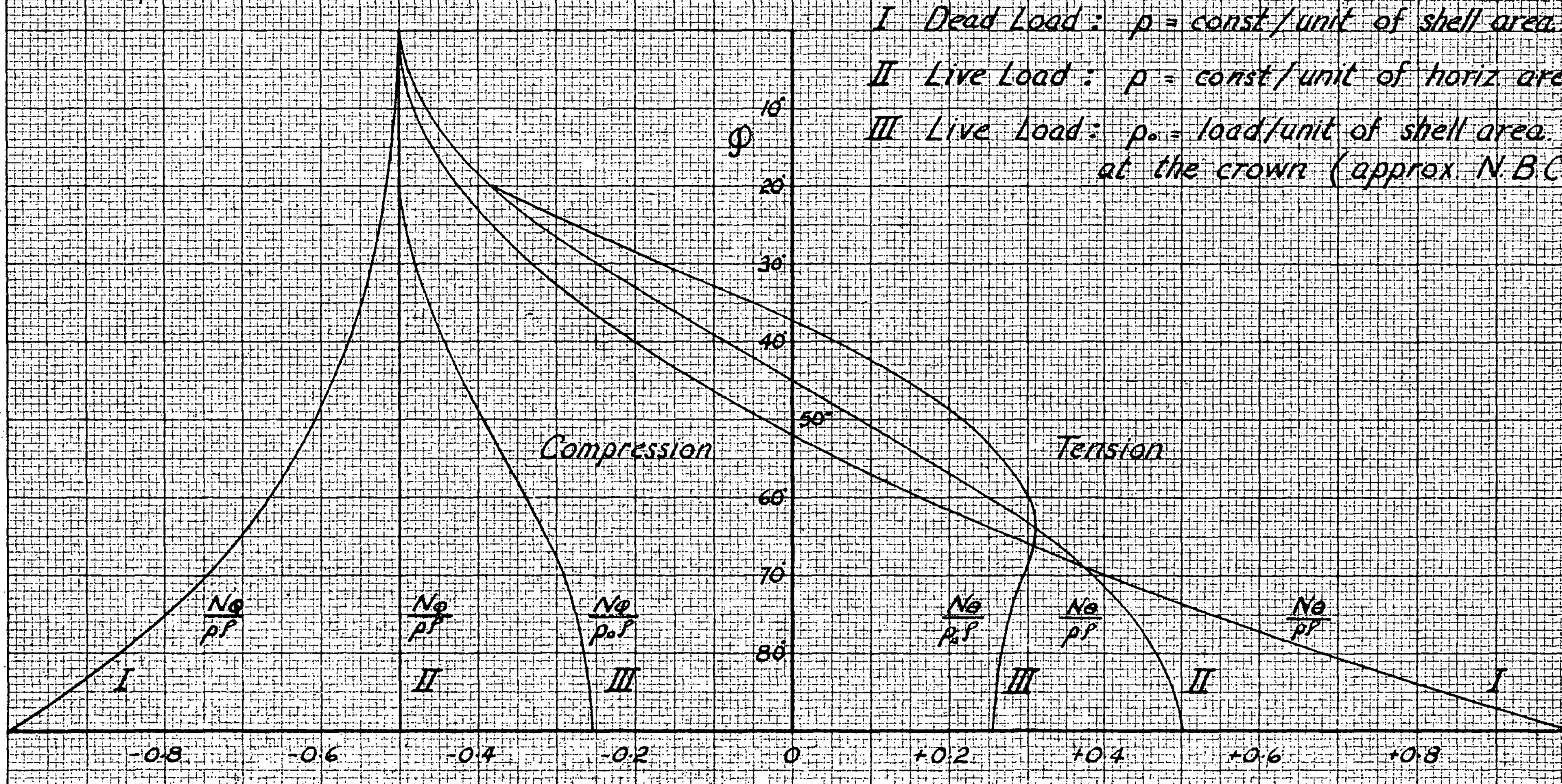

Graph 1 - 1

2. Spherical Shell under Live Load, constant per unit of Horizontal Area.

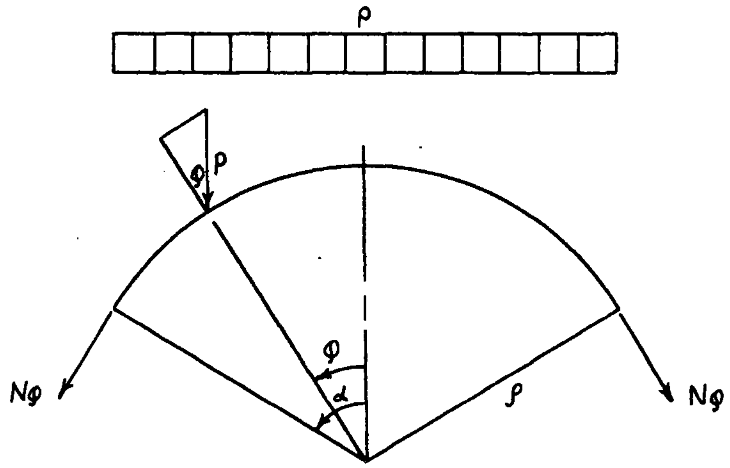

Fig (1 - 6)

The horizontal area over which the load acts is $\pi \ (\rho \sin\varphi)^2$

The load on the shell is then

$$R = \pi p \rho^2 \sin^2\varphi \qquad (1 - 7)$$

Substituting R into Equation (1 - 2) gives

$$N\varphi = - \frac{p\rho}{2} \qquad (1 - 8)$$

Substituting Equation (1 - 8) into Equation (1 - 1) gives

$$N\theta = \frac{p\rho}{2} \ (1 - 2\cos^2\varphi) \qquad (1 - 9)$$

$$= - \frac{p\rho}{2} \cos 2\varphi$$

Equations (1 - 8) and (1 - 9) are also plotted in Graph 1 - 1

In reality, a snow load of the form just discussed is not obtained because the snow does not hold to the steeper pitches. The National Building Code of Canada (1953) gives a constant snow load for slopes up to twenty degrees. Thereafter the load drops off linearly to zero at sixty-three degrees. The expression

$$p = p_o \frac{\cos\varphi - \cos 65^\circ}{\cos 20^\circ - \cos 65^\circ} \qquad (1 - 10)$$

for $20^\circ \leq \varphi \leq 65^\circ$, where p_o is the load on a flat surface, gives a snow load distribution slighttly heavier than the National Building Code. For $\varphi \leq 20^\circ$, Equations (1 - 8) and (1 - 9) apply. For $\varphi > 20^\circ$, Equation (1 - 10) is integrated to obtain the part of the load on the shell where $\varphi > 20^\circ$ and is added to the load on the shell for $\varphi \leq 20^\circ$, giving the total load. Equations (1 - 1) and (1 - 2) then give the membrane forces. The membrane forces are also plotted in Graph 1 - 1.

C. SHELL OF REVOLUTION, UNSYMMETRICAL LOAD.

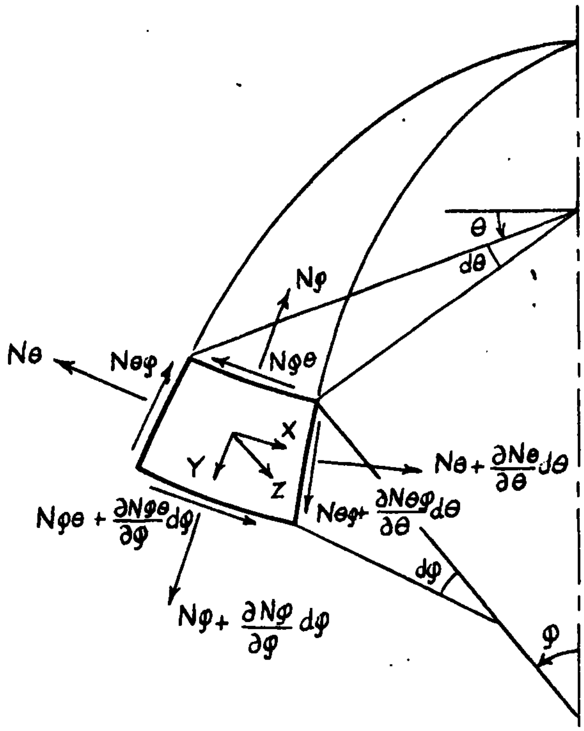

Fig 1 - 7

In the case of an unsymmetrical load, not only normal forces N_φ and N_θ but also shear forces $N_{\varphi\theta}$ and $N_{\theta\varphi}$ act on the element as shown in Figure (1 - 7). Equating the sum of the moments about the axis to zero gives $N_{\varphi\theta} = N_{\theta\varphi}$ and reduces thereby the number of unknowns to three. Equating to zero the sum of the projections on the three co-ordinate axes gives the three equations

$$\left.\begin{aligned}
&\frac{\partial}{\partial\varphi}(N_\varphi\, r) + \frac{\partial N_{\theta\varphi}}{\partial\theta}\, r_1 - N_\theta\, r_1 \cos\varphi + Y r_1 r = 0 \\
&\frac{\partial}{\partial\varphi}(r\, N_{\varphi\theta}) + \frac{\partial N_\theta}{\partial\theta}\, r_1 + N_{\theta\varphi}\, r_1 \cos\varphi + X r_1 r = 0 \\
&\frac{N_\varphi}{r_1} + \frac{N_\theta}{r_2} = -Z
\end{aligned}\right\} \quad (1\text{-}11)$$

These three partial differential equations involving the three unknowns N_φ, N_θ and $N_{\theta\varphi}$ can be solved in the general case by expanding both the load and the stresses in trigonometric series.[2] The following section gives the solution for a wind pressure on a spherical shell.

2. W. Flugge, Stafik und Dynamik der Schalen, Berlin, 1934.

1. SPHERICAL SHELL UNDER WIND LOAD.

The National Building Code does not specify any wind pressure on domes. However a loading can be assumed which basically follows the findings of the National Building Code. Wind pressure acts normal to the surface and increases the pressure on the windward side and decreases the pressure or causes suction on the leeward side. If the direction of the wind is in the meridian plane $\theta = 0°$

then $X = Y = 0$, $Z = p \sin\varphi \cos\theta$ (1 - 12)

Where P is the wind pressure on a vertical surface. Equation 1 - 13 gives a distribution as shown in Fig 1 - 8

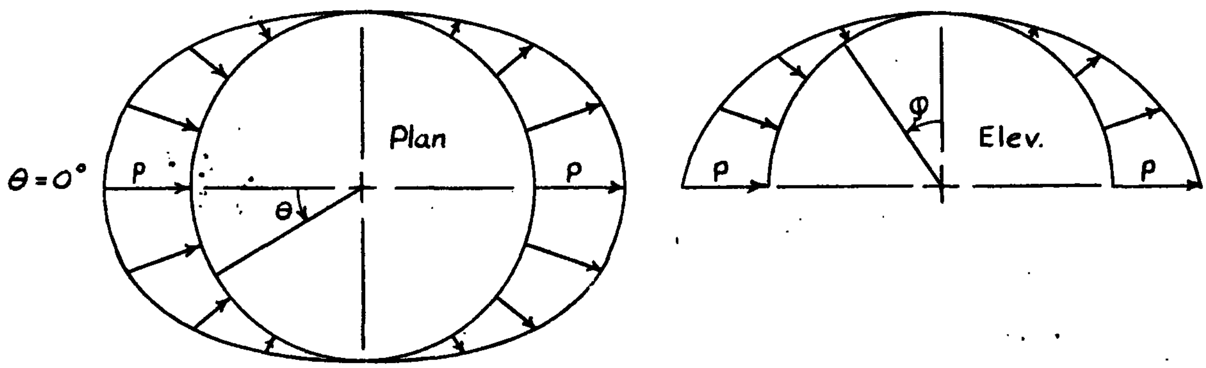

Fig (1 - 8)

The solution to Equations (1 - 11) is given by

$$N_\varphi = -\frac{p\rho}{3}\,\frac{\cos\theta\cos\varphi}{\sin^3\varphi}\left(2 - 3\cos\varphi + \cos^3\varphi\right) \qquad (1-13)$$

$$N_\theta = -\frac{p\rho}{3}\,\frac{\cos\theta}{\sin^3\varphi}\left(-2\cos\varphi + 3\sin^2\varphi + 2\cos^4\varphi\right) \qquad (1-14)$$

$$N_{\theta\varphi} = -\frac{p\rho}{3}\,\frac{\sin\theta}{\sin^3\varphi}\left(2 - 3\cos\varphi + \cos^3\varphi\right) \qquad (1-15)$$

Inspection of these equations show that the normal forces have a maximum compressive value at $\theta = 0^\circ$ and a maximum tensile value at $\theta = 180^\circ$. The shear forces, however, attain a maximum value at $\theta = 90^\circ$ and $\theta = 270^\circ$. The maximum and minimum values of the forces due to wind pressure may be obtained from Graph 1 - 2 for a given value of φ. The resulting stresses due to wind action may then be superimposed over those resulting from dead and live loads.

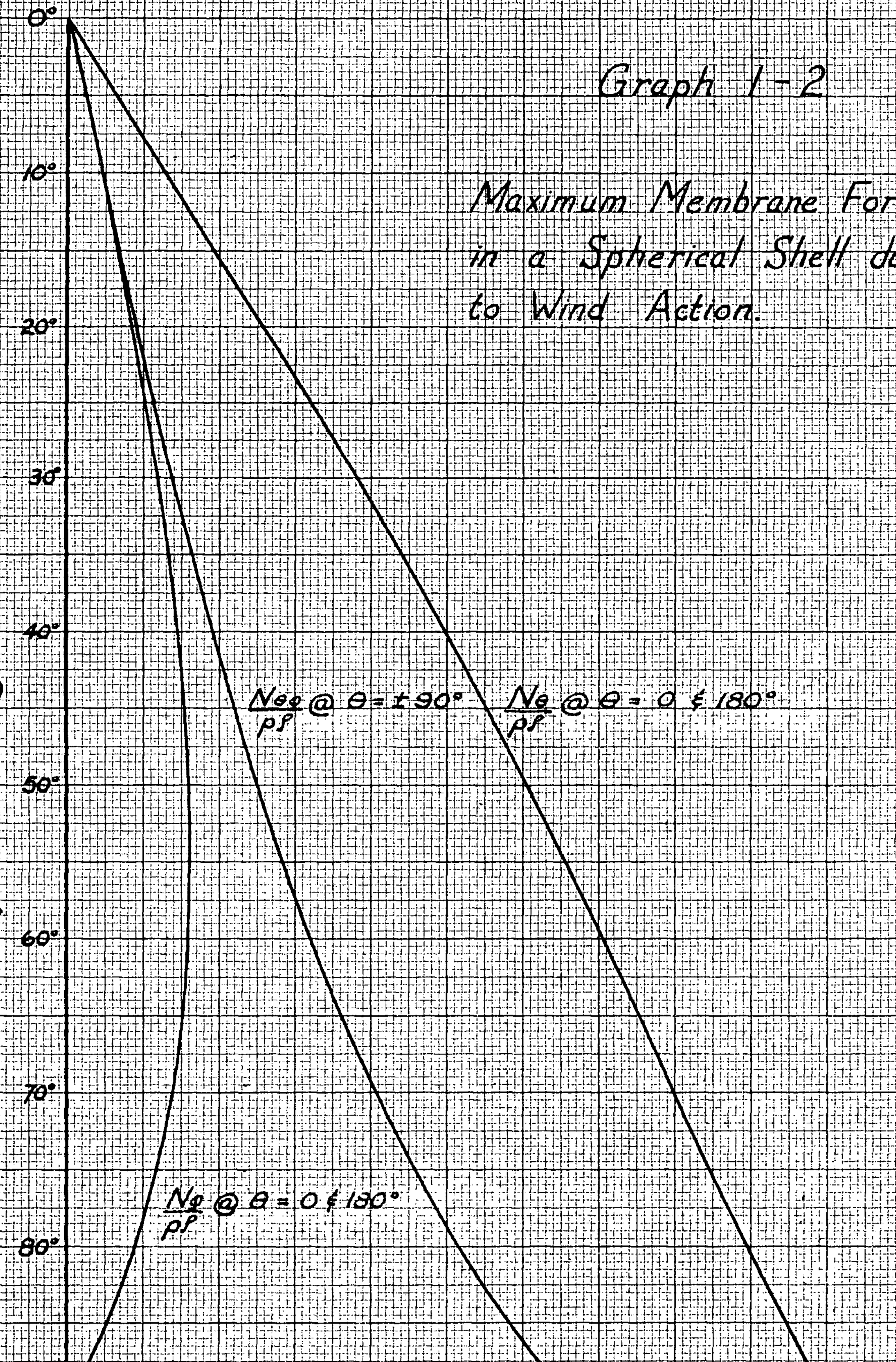

Graph 1-2

Maximum Membrane Forces in a Spherical Shell due to Wind Action.

CHAPTER II

GEOMETRY

A. INTRODUCTION

Since shells of revolution have curvature in two directions, their usage is restricted to those materials which can be moulded to the appropriate curvatures. This limitation permits the use of concrete, steel and aluminum. Unfortunately, concrete entails the use of an elaborate formwork and steel and aluminum each require a costly pressing process.

A structure composed of flat plates closely approximating a shell of revolution possesses some advantages over a continuous shell. The formwork is simpler and the pressing process is eliminated. Such a structure may be fabricated with comparative ease from a good grade of plywood. The following section develop the geometry of such a shell which is called a geodesic or folded plate shell.

The economy of a folded plate shell is improved by minimizing the number of different plate shapes involved. Since a sphere has an infinite number of axes of symmetry, a spherical shell probably has fewer shapes than any other shell of revolution that might be approximated with flat plates.

We will deal only with triangular shapes since they are easier to fabricate and are stronger area for area than other shapes that might be used, such as: quadrilaterals, pentagons and hexagons.

B. BASIC GEOMETRY.

The five basic polyhedra that can be inscribed in a sphere are the tetrahedron, cube, octahedron, dodecahedron and icosahedron.[1] The icosahedron is composed of twenty equilateral triangles and the dodecahedron, of twelve pentagons. Since the icosahedron and dodecahedron have more facets, they more nearly approximate a spherical shell than do the other three polyhedra. For that reason, the icosahedron and dodecahedron are the better polyhedra to use as a basis for developing the geometry of a geodesic shell.

The standard size of plywood sheet is four feet by eight feet. Some mills produce sheets forty or fifty feet long and extra width sheets may also be ordered. Generally, the four foot width governs the maximum size of triangle. Therefore, to obtain a practical sized shell, it is necessary to subdivide the triangles and pentagons of the icosahedron and dodecahedron respectively into smaller structural elements.

[1] H. M. Cundy and A. R. Rollett, <u>Mathematical Models</u> Oxford University Press, 1952.

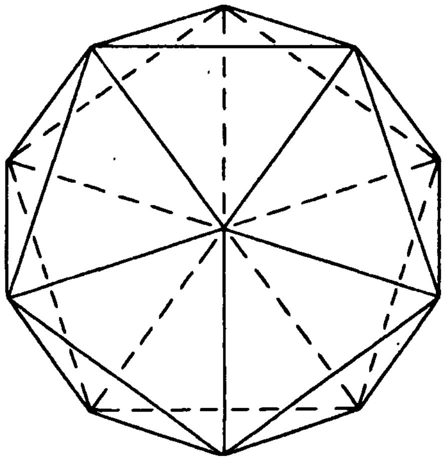

Fig 2 - 1 Icosahedron

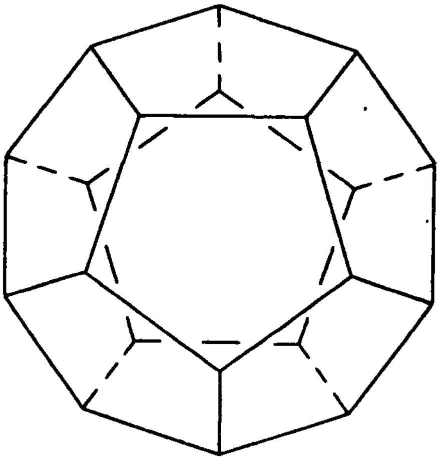

Fig 2 - 2 Dodecahedron

It is not merely a case of breaking up the triangles and pentagons in their own plane but rather of moving the newly formed vertices radially to the circumscribing sphere. This procedure gives a closer approximation of a sphere than does the basic polyhedra. There are numerous ways of subdividing a triangle and since the computations are rather time consuming, only a few methods of subdivision have been investigated. For that reason, there may be other methods of subdivision that are more advantageous for a specific radius and material than those given here.

The icosahedron is first subdivided by bisecting the sides of the equilateral triangle and moving the newly formed points radially to the circumscribing sphere. As shown in Fig. 2 - 3, one equilateral triangle of the icosahedron is replaced by four triangles, one equilateral and three isosceles. Since the isosceles triangles are congruent by symmetry, there are only two kinds of triangles. A sphere is now approximated by 80 triangles instead of 20 triangles as in the icosahedron.

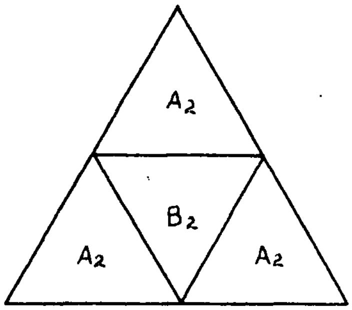

Fig 2 - 3

Instead of dividing the side of the equilateral triangle into two parts, the side can be divided into three parts. One equilateral triangle of the icosahedron is now replaced by nine smaller triangles with each new vertex displaced radially to touch the circumscribing sphere. A general subdivision, by trisecting the sides of the equilateral triangle for example, gives three kinds of isosceles triangles as shown in Fig 2 - 4a.

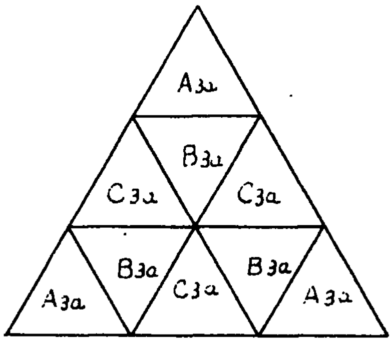

Fig 2 - 4 a

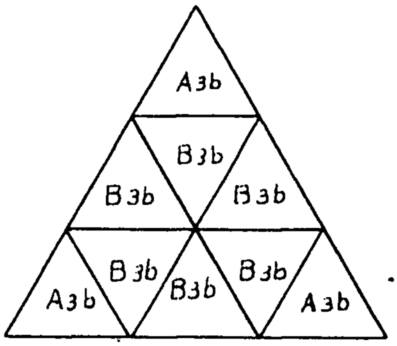

Fig 2 - 4 b.

Instead of trisecting the sides, it is possible to prescribe that two kinds of isosceles triangles be congruent to each other. If the triangle is subdivided, making triangles B 3a and C 3a congruent, a subdivision is obtained as shown in Figure 2 - 4 b. Thus a sphere is approximated with 180 triangles of two kinds.

Working from Figure 2 - 3, the sides of the icosahedron triangle may be divided into four parts. By prescribing congruency, triangle A 2 of Figure 2 - 3 can be subdivided into four triangles of two kinds, A4 isosceles and B4 scalene as shown in Fig. 2 - 5. Triangle B2 also breaks up into four triangles of two kinds, C4 equilateral and D4 isosceles. The result of the breakdown is shown in Fig 2 - 5. A sphere is approximated by 320 triangles of four kinds.

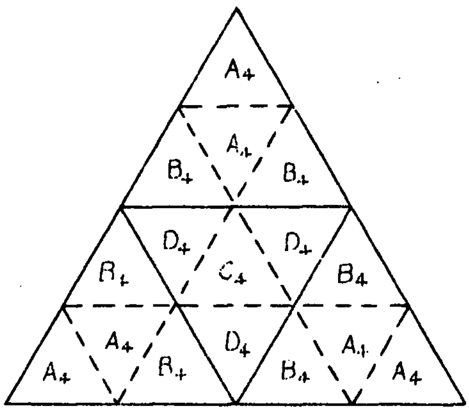

Fig 2 - 5

Working from Figure 2 - 5, the triangles may again be subdivided. It does not appear possible to prescribe any congruency among the triangles obtained by subdividing the scalene triangle B4, so that four kinds of triangles are formed. As before the isosceles and equilateral triangles can each be broken down into two kinds of triangles. Therefore a sphere is approximated by 1280 triangles of ten kinds. (Figure 2 - 6)

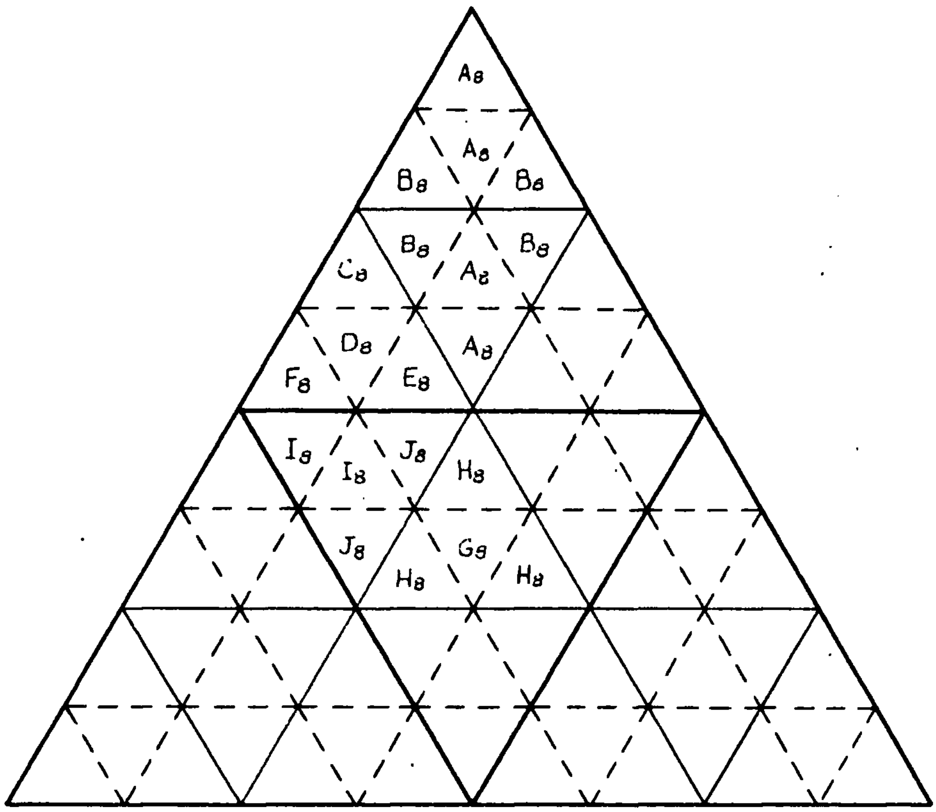

Fig 2 - 6

Figure 2 - 4b can also be subdivided in the same manner Fig 2 - 3 was subdivided. The subdivision may be carried out indefinitely. Unfortunately, once a number of scalene triangles appear in the subdivision, the number of kinds of triangles grow rapidly. For example, Fig 2 - 6 has ten kinds of triangles but one further subdivision of this figure has 32 kinds of triangles. However, considering that in this case there are 5120 triangles in a sphere, 32 kinds of triangles are not unreasonable.

The subdivision of the dodecahedron is indicated in Figure 2 - 7. A sphere is formed in (b) by 60 triangles of one kind, in (c) by 240 triangles of two kinds and in (d) by 960 triangles of six kinds. One further subdivision, not illustrated forms a sphere of 3840 triangles of 22 kinds.

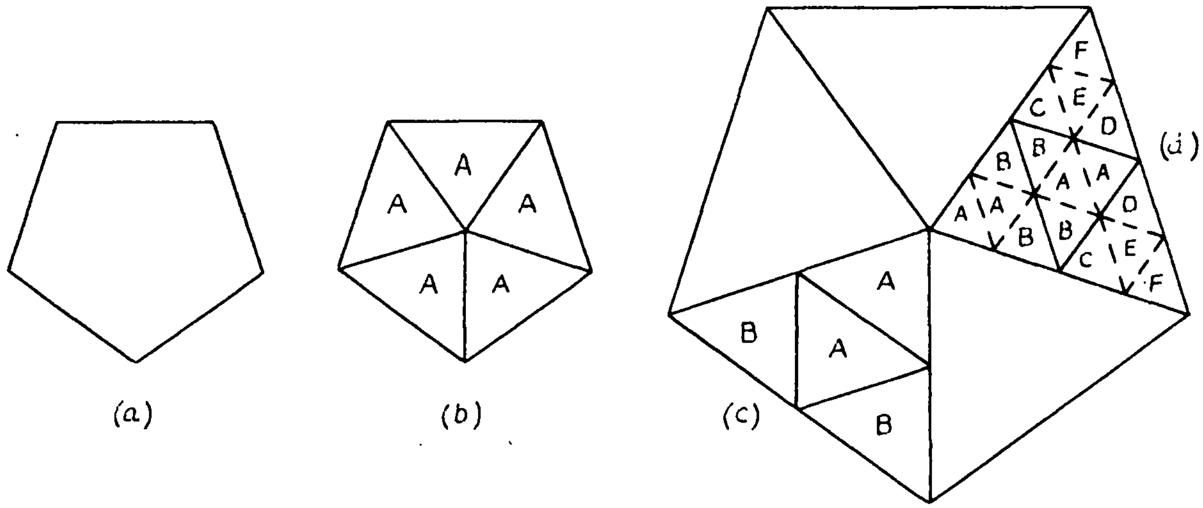

Fig 2 - 7

The various subdivisions indicated in the preceding paragraphs all yield triangles that are nearly equilateral. A one piece triangle of plywood therefore has an altitude of approximately four feet and an area of 7.6 square feet. The total number of triangles required to replace a spherical segment is approximately equal to the spherical area divided by 7.6. Graph 2 - 1 shows these results. For a given span and rise, the graph gives the radius, the total number of triangles denoted by Nt and also the approximate number of kinds of triangles denoted by Nk. These parameters then act as a guide to the choice of the appropriate subdivision.

Span (L) and Height (H) for Spherical Segments made from Given Numbers of Triangles (N_T) and Radius (ρ) for an Average Area of 7.6 sq. ft. per Triangle.

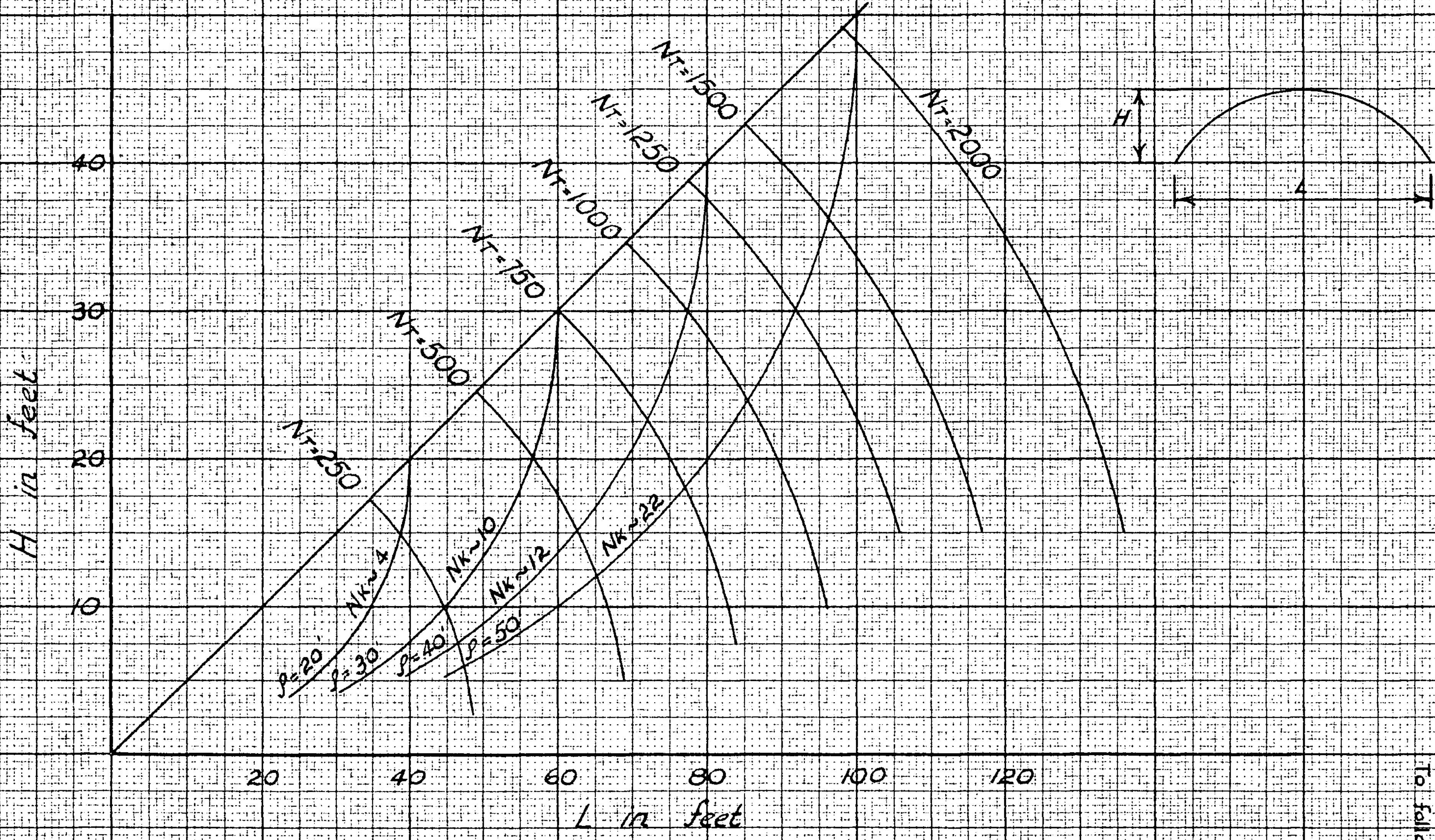

Graph 2-1

To follow 21

Another type of subdivision may be visualized by referring back to Figure 2 - 4b which has nine isosceles triangles of two kinds. The perpendicular bisector of the base breaks each isosceles triangle into two congruent parts even though the newly formed vertex is raised to the circumscribing sphere. Therefore the sphere is approximated by 360 triangles of only two kinds. The triangles are now more nearly 30-60-90 instead of equilateral and may be obtained from a four by eight sheet of plywood by cutting diagonally. From a structural point of view, this shape of triangle is not as good as the equilateral shape. The membrane forces are affected by the large variation of the dihedral angles. Also, the triangle may have to be stiffened to minimize bending and prevent buckling. The battens connecting the long sides together may also be heavier.

C. METHOD OF CALCULATION

The triangle geometry is best solved by using trigonometry. The sphere is first divided into spherical triangles which are then replaced by the corresponding plane triangles. The side of the spherical triangle is in angular arc, Ψ . Reference to Figure 2 - 8 shows that the corresponding length of the side of the plane triangle is $2 \rho \sin \frac{\Psi}{2}$.

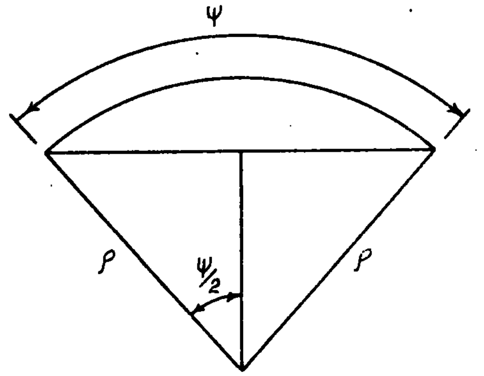

Fig 2 - 8

The dihidral angles are solved by using analytical geometry. In Figure 2 - 9, it can be proved that the angle between the triangle plane a b c and the Plane o a b, is obtained from

$$\lambda = \tan^{-1}\left(\frac{\sqrt{2(1+\cos\gamma)(\sin^2\gamma - \cos^2\alpha - \cos^2\beta + 2\cos\alpha\cos\beta\cos\gamma)}}{\sin\gamma(1+\cos\gamma - \cos\alpha - \cos\beta)}\right) \qquad (2-1)$$

Where O is the centre of the sphere and α, β, γ are the angles shown. α and β are interchangeable

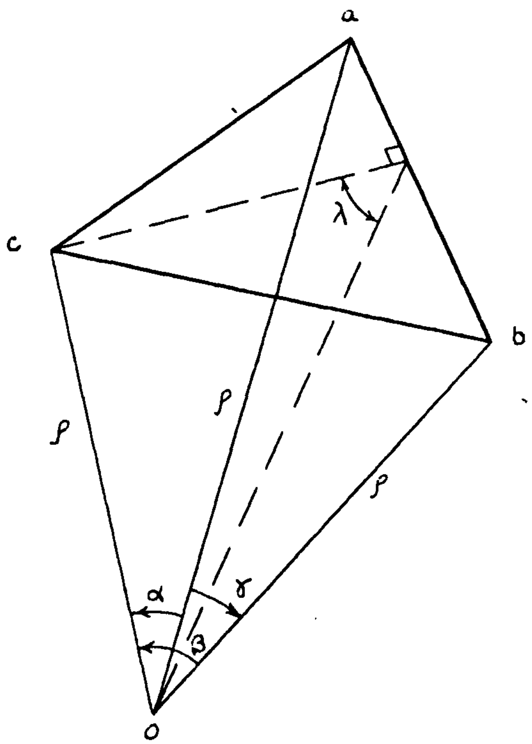

Fig 2 - 9

in this formula but γ is not. The last term under the square root sign is close to zero so it must be evaluated accurately. However for the angles involved,

$\tan \lambda$ approaches infinity so the formula gives accurate results. Formula (2 - 1) must be evaluated once for each triangle on either side of the plane o a b. The dihedral angle is then the sum of the two values of λ.

The geometry for some of the subdivisions has been computed and the results presented in tabular form. The trigonometry was calculated to the nearest second of arc using six place natural functions and a desk calculator. The results therefore should be good to five significant figures.

The fabricator should cut the triangles as precisely as the material and equipment permit if the structure is to fit properly together. If the dome is fabricated in sections, the triangle geometry of an appropriate coarser subdivision gives chord distances which may be used to check the fabricated section.

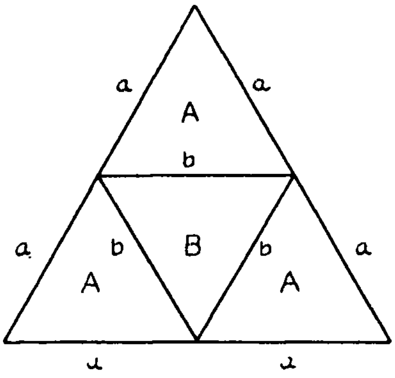

Table 2 - 1

$\triangle$	Sides	Req'd. for Sphere	Side	Arc	Length / ρ	Edge	180°- Dihedral Angle
A	a a b	60	a	a = 31° 43' 03"	.54652	A a A	22° 14'
B	b b b	20 / 80	b	b = 36° 00' 00"	.61804	A b B	18° 00'

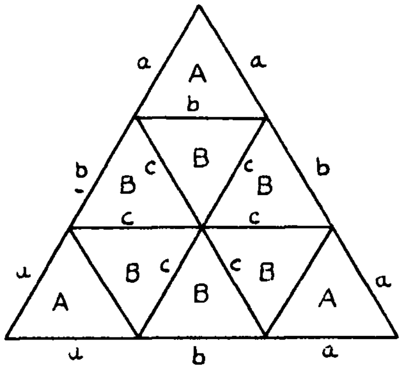

Table 2 - 2

$\triangle$	Sides	Req'd. for Sphere	Side	Arc	Length / ρ	Edge	180°- Dihedral Angle
A	a a b	60	a	a = 20° 04' 36"	.34861	A a A	14° 34'
B	c c b	120	b	b = 23° 16' 54"	.40358	A b A	11° 22'
		180	c	c = 23° 46' 02"	.41247	B b B	14° 28'
						B c B	11° 34'

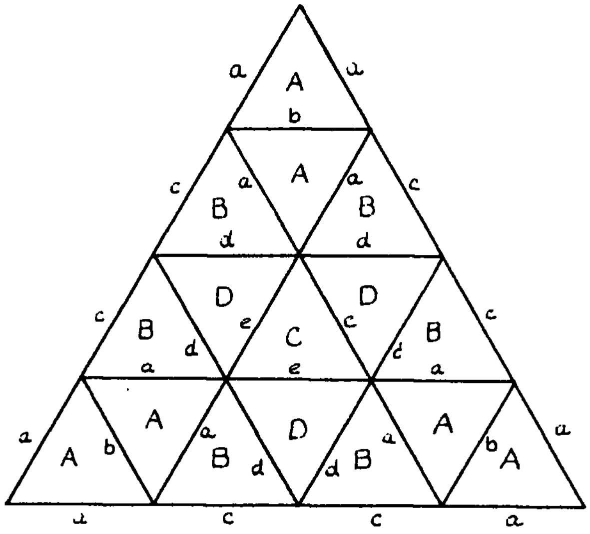

Table 2 - 3

Δ	Sides	Req'd. for Sphere	Side	Arc	Length ρ	Edge	180°- Dihedral Angle
A	a a b	120	a	a = 16° 16' 01"	.282959	A a A	11° 44'
B	a c d	120	b	b = 18° 57' 12"	.329292	A b A	6° 32'
C	e e e	20	c	c = 15° 27' 02"	.268857	A a B	11° 04'
D	d d e	60	d	d = 18° 00' 00"	.312869	B c B	11° 38'
		320	e	e = 18° 41' 58"	.324920	B d D	9° 00'
						D e C	10° 21'

Table 2-4

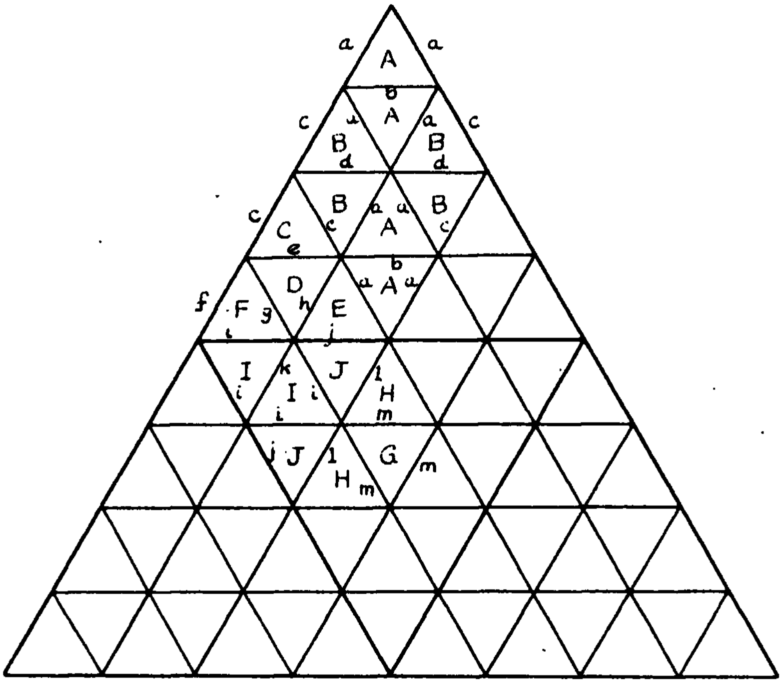

Δ	Sides	Req'd. for Sphere	Side	Arc	Length / ρ	Edge	180°-Dihedral Angle
A	a a b	240	a	8° 11' 23"	.142816	A a A	5° 56'
B	a c d	240	b	9° 36' 22"	.167462	A b A	3° 10'
C	c c e	120	c	8° 04' 38"	.140858	A a B	5° 51'
D	e g h	120	d	9° 28' 36"	.165211	A a E	5° 31'
E	a h j	120	e	9° 13' 14"	.160756	B c B	5° 55'
F	f g i	120	f	7° 22' 24"	.128600	B d B	3° 14'
G	m m m	20	g	8° 07' 01"	.141549	B c C	5° 46'
H	l l m	60	h	7° 46' 56"	.135721	C c C	5° 37'
I	i i k	120	i	9° 03' 38"	.157972	C e D	3° 20'
J	i j l	120	j	8° 56' 22"	.155865	D h E	5° 48'
		1280	k	9° 29' 53"	.165583	D g F	5° 14'
			l	9° 20' 59"	.163002	E j J	4° 37'
			m	9° 26' 40"	.164650	F f F	6° 20'
						F i I	4° 20'
						G m H	5° 18'
						H l J	5° 11'
						J k I	5° 22'
						I k I	4° 48'

CHAPTER III

THEORETICAL ANALYSIS

A. INTRODUCTION

In the analysis of folded plate shells, the designer must consider membrane stress, bending stress and stability. The membrane stress, as will be shown later, may be obtained from smooth shell theory. Bending stresses arise mainly from loads perpendicular to the surface of the triangle.

Failure of a structure may be caused not only by high stresses but also by instability. In geodesic shells, buckling may occur in two ways. The dome as a unit may buckle or an individual triangle may buckle. While the latter case is due to local instability it could be sufficient to bring about complete failure.

The following sections consider in more detail these aspects to be considered in design and analysis. While only spherical shaped shells are considered, the concepts apply also to other shaped shells of revolution.

B. MEMBRANE STRESS

The exact solution of the membrane stresses in a folded plate shell is a statically indeterminate problem. Special types of folded plate domes, such as Polygonal Domes,[1] have an exact solution in terms of tabulated functions. Unfortunately, the exact solution of the folded plate shell considered here does not appear in terms of tabulated functions. For this reason, it was decided to apply an approximate solution using smooth shell theory.

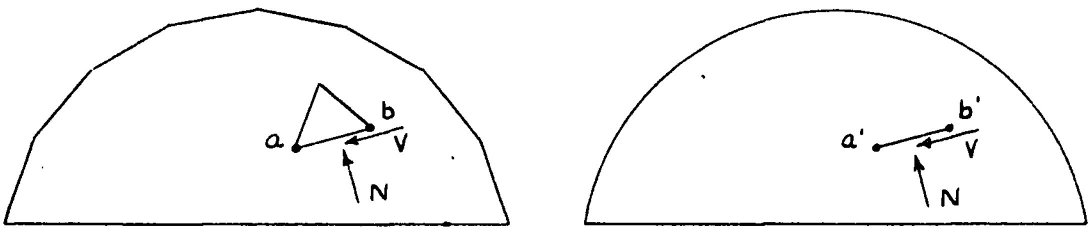

Fig 3 - 1

If the geodesic shall is compared to a smooth shell of the same radii, then the load on the triangle edge ab (Figure 3 - 1) is the same as the load on the corresponding arc a'b' of the smooth shell.

[1] W. Flugge, Statik und Dynamil der Schalen, Berlin, 1934

The validity of applying smooth shell theory to geodesic shells is shown by considering the geometry and behaviour under load of the two types of shell. It was shown in Chapter I that loads on a smooth shell are supported by membrane action. These membrane stresses are indicated qualitatively in Figure 3 - 2, a and b. The corresponding geodesic shell is shown in Figure 3 - 2, c and d. The geodesic shell is a doubly curved structure as is the smooth shell and both have little bending resistance. Therefore the only way loads can be carried in either shell is by direct stress.

Figure 3 - 2 c is the cross section of a segment of the polyhedron having only 320 triangles approximating a sphere. Even this apparently coarse approximation of a sphere is not far from the true sphere. Some radius $\rho - \Delta\rho$ passes half way between the inner and outermost points on the triangles approximating the sphere. $\Delta\rho$ is a very small percent of ρ and becomes even smaller as the number of triangles in the complete polyhedron increase. Therefore the co-ordinates of the polyhedron are virtually the same as those of the sphere.

Equating the sum of the vertical forces to zero in figures (a) and (c) show that N_φ must be the same for both cases since the loads are supported only by direct stress. Similarly in figures (b) and (d), equating the sum of the horizontal forces to zero show that the total force in the θ direction is the same in both cases. Therefore the total forces acting on the isolated segments in figures (e) and (f) are the same. Equating moments to zero about the point O show that the general distribution of N_θ must be the same in both cases. Since the geometry and membrane forces are practically the same for both shells, the application of smooth shell theory is justified.

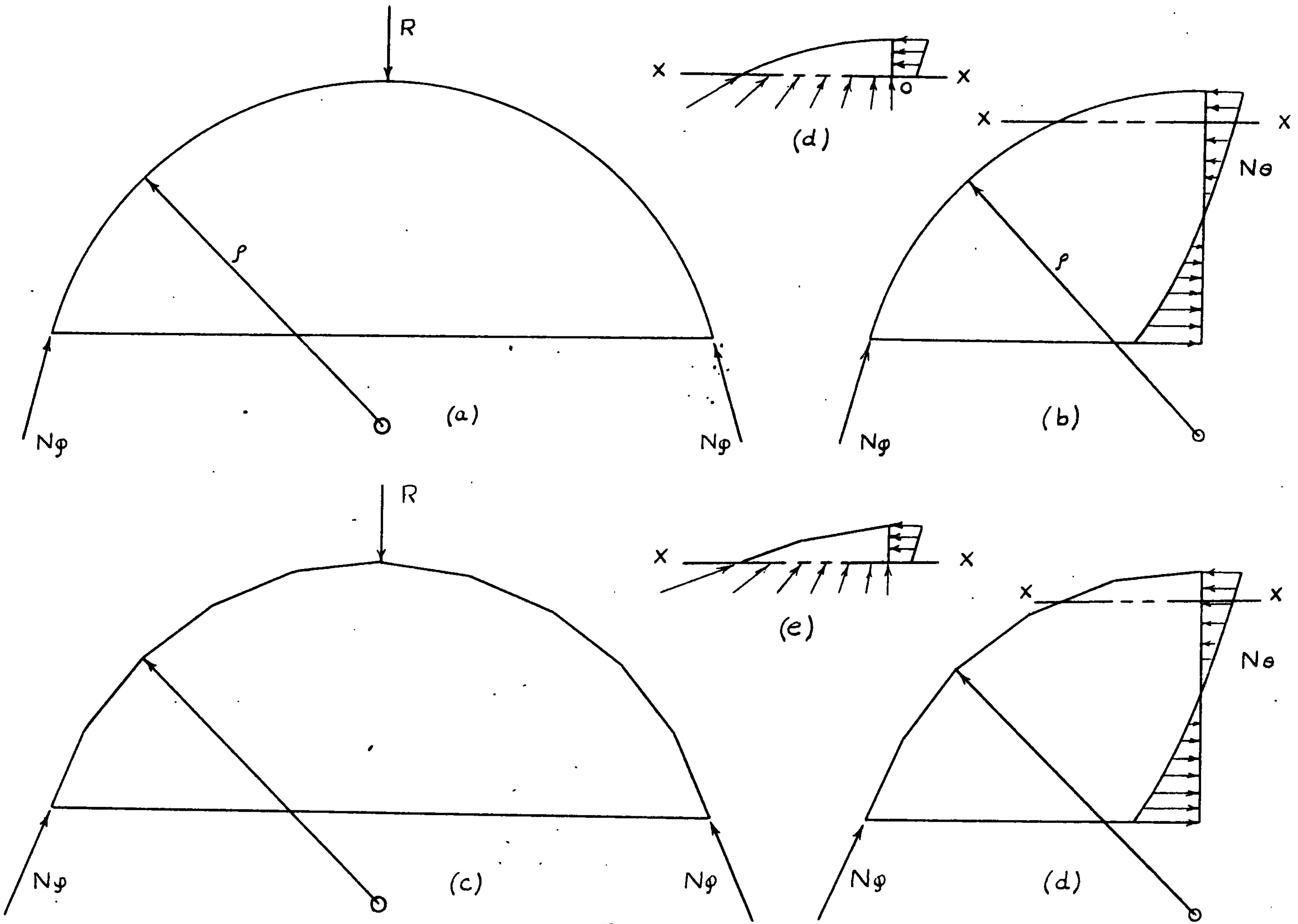

Fig. 3-2

To follow p 30

Applying smooth shell theory to geodesic shells gives a near uniform distribution of membrane stress along the edge of a triangle. This is not true because the deformations along the edge cause a redistribution of stress but the total load remains the same. Consider the common edge e of two triangular plates under membrane action as shown in Fig 3 - 3 a. By action and reaction, at the edge e the direction of stress σ is at angle β to each plate. The component

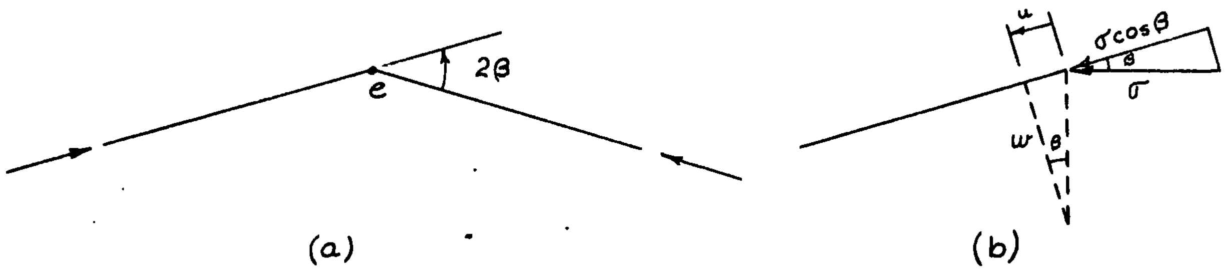

Fig 3 - 3

in the plane of the plate causes deformation u. To preserve continuity along the common boundary, the plate must also bend with a deflection w. The effect is to redistribute the membrane stress into a parabolic shape with the highest stresses at the corners of the triangle. Therefore smooth shell theory gives the average stress on the triangle edge but not the maximum stress.

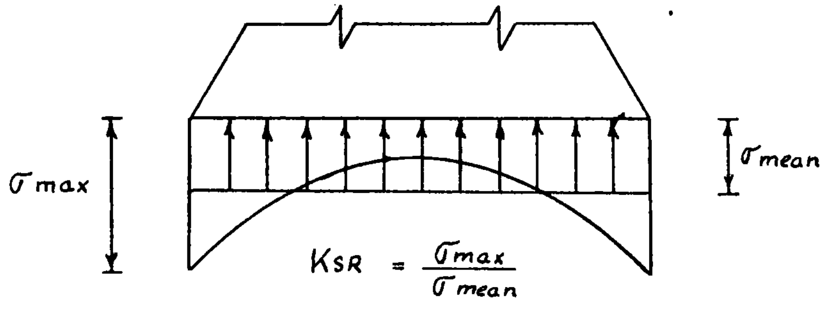

Fig 3 - 3 (c)

To evaluate the maximum membrane stress, the stress riser at the corners must be determined. It might be determined by a Fourier analysis of two isolated triangles, preserving continuity along the common boundary. However the lack of convenient tabulated functions made this approach impractical. Instead of isolating two triangles, two rectangles were isolated and a Fourier analysis attempted. However a stress function for the membrane action was not obtained which satisfied both the boundary condition and continuity. Because of this, it was decided to find the stress riser by experiment. The results of the experimental work are found in Chapter IV. The experimental work does show that smooth shell theory can be used with a stress riser for the corners.

C. BENDING OF A TRIANGLE UNDER UNIFORM NORMAL PRESSURE.

The differential equation of a plate under a normal pressure q is[2]

$$\nabla^4 w = \frac{\partial^4 w}{\partial x^4} + 2\frac{\partial^4 w}{\partial x^2 \partial y^2} + \frac{\partial^4 w}{\partial y^4} = \frac{q}{D} \qquad (3-1)$$

where w is the deflection at a point with co-ordinates x and y and $D = \frac{Eh^3}{12(1-\mu^2)}$ is the flexural rigidity of the plate. This expression is based on the small deflection theory where the deflection is small compared to the thickness. As long as the deflections are small, the membrane forces, by beam column action, have a very small effect on the actual deflection and may be omitted from the discussion. That comparatively small deflections do occur may be verified by calculating the maximum deflection and comparing it to the plate thickness.

[2] S. Timoshenko, Theory of Plates and Shells, New York, McGraw-Hill, 1940, P. 88.

The solution of Equation 3 - 1 involves the determination of some function for w which not only satisfies this differential equation but also the boundary conditions. For a simply supported plate, the deflection and bending moments must be zero at the plate edges. Therefore the boundary conditions are

$$w = 0 \tag{3 - 2}$$

and

$$\frac{\partial^2 w}{\partial n^2} = 0 \tag{3 - 3}$$

at the edges where n is the co-ordinate axis perpendicular to the edge. Expressing Equation 3 - 3 in terms of x and y for convenience only, the boundary condition becomes instead

$$\frac{\partial^2 w}{\partial x^2} + \frac{\partial^2 w}{\partial y^2} = 0 \tag{3 - 4}$$

A general satisfactory expression for w for any shape of triangular plate is not in terms of tabulated functions. A few specific cases are tabulated however. One such case is for a simply supported equilateral triangle under uniform lateral load[3]. For the type of dome considered here, all the triangles are very nearly equilateral. Therefore the bending stresses may be closely approximated by considering only an equilateral triangle.

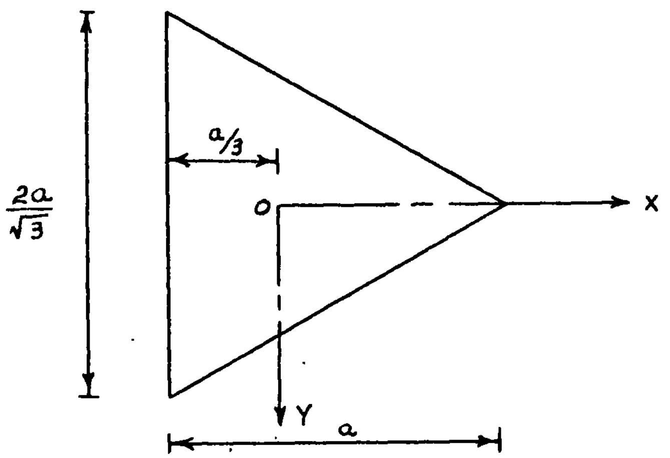

Fig 3 - 4

[3] The bending of an equilateral plate was solved by S. Woinowsky - Krieger, Ingenieur - Archiv., vol.4, p.254

With co-ordinate axes as shown in Figure 3 - 4, the deflection surface of a uniformly loaded, simply supported, equilateral triangle is [4]

$$w = \frac{q}{64aD}\left[x^3 - 3y^2 x - a(x^2 + y^2) + \frac{4}{27}a^3\left(\frac{4}{9}a^2 - x^2 - y^2\right)\right] \quad (3 - 5)$$

The part of the polynomial in square brackets is the product of the left hand side of

$$x + \frac{a}{3} = 0$$

$$\frac{x}{3} + y - \frac{2a}{3\ 3} = 0$$

$$\frac{x}{3} - y - \frac{2a}{3\ 3} = 0$$

which are the equations of the boundary lines. The expression in square brackets is therefore zero at the boundary. Hence the boundary condition, $w = 0$, is satisfied. Successive differentiation of the polynomial gives

$$\frac{\partial^2 w}{\partial x^2} + \frac{\partial^2 w}{\partial y^2} = -\frac{q}{4aD}\left[x^3 - 3y^2\ x\ \ 3y^2\ x - a(x^2 + y^2) + \frac{4}{27}a^3\right] \quad (3 - 4a)$$

and

$$\frac{\partial^4 w}{\partial x^4} + 2\frac{\partial^4 w}{\partial x^2 y^2} + \frac{\partial^4 w}{\partial y^4} = \frac{q}{D} \quad (3 - 1)$$

Similarly, Equation 3 - 4a is also zero at the boundary so that both boundary conditions are satisfied. The differential equation is also satisfied. Therefore

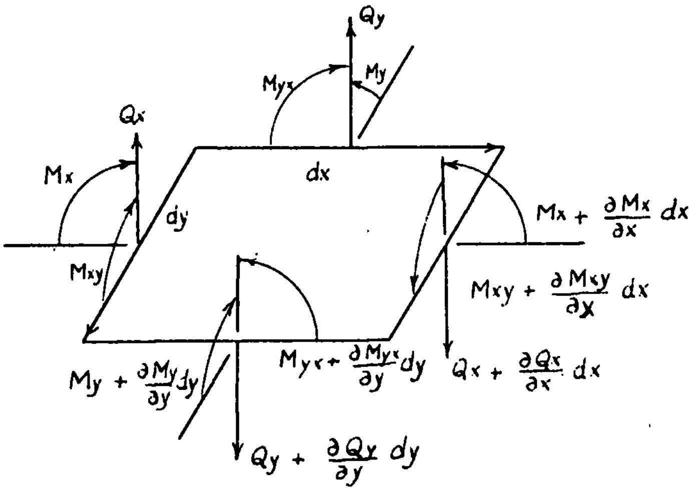

Fig 3 - 5

4 S. Timoshenko, <u>Theory of Plates and Shells</u>
New York, McGraw-Hill, 1940, p.293

Equation 3 - 5 represents the solution for the deflection surface. The maximum deflection occurs at the centroid of the triangle and is

$$w_{max} = \frac{q\, a^4}{3888\; D} \tag{3-6}$$

The differential equations for the moments, as defined in Figure 3 - 5, are

$$Mx = -D\left(\frac{\partial^2 w}{\partial x^2} + \mu \frac{\partial^2 w}{\partial y^2}\right)$$

$$My = -D\left(\frac{\partial^2 w}{\partial y^2} + \mu \frac{\partial^2 w}{\partial x^2}\right) \tag{3-7}$$

$$Mxy = -Myx = D\,(1-\mu)\,\frac{\partial^2 w}{\partial x\,\partial y}$$

Therefore

$$Mx = -\frac{q}{16\,a}\Big[-(5-\mu)\,x^3 + (3+\mu)\,ax^2 + \frac{2}{3}\,(1-\mu)\,a^2x - \frac{8}{27}\,(1+\mu)\,a^3$$

$$+\,3\,(1+3\mu)xy^2 + (1+3\,\mu)\,ay^2\Big] \tag{3-8}$$

$$My = -\frac{q}{16\,a}\Big[(1-5\mu)\,x^3 + (1+3\mu)ax^2 - \frac{2}{3}\,(1-\mu)\,a^2x - \frac{8}{27}\,(1+\mu)a^3$$

$$+\,3(3+\mu)xy^2 + (3+\mu)\,ay^2\Big] \tag{3-9}$$

and

$$Mxy = \frac{q\,(1-u)}{16\,a}\left[3x^2y + 2\,axy - \frac{2}{3}\,a^2y + 3\,y^3\right] \tag{3-10}$$

All the terms in Equation 3 - 10 contain y so Mxy is zero along the x axis. Setting the partial derivatives of Mx and My with respect to y equal to zero and solving shows that the only valid solution is for y = 0. Therefore Mx and My are a maximum along the x axis. Equating y to zero and introducing the notation $S = \frac{x}{a}$, the moment equations become

$$M_x\Big]_{y=0} = \frac{qa^2}{16}\left[(5-\mu)S^3 - (3+\mu)S^2 - \frac{2}{3}(1-\mu)S + \frac{8}{27}(1+\mu)\right] \tag{3-11}$$

$$M_y\Big]_{y=0} = \frac{qa^2}{16}\left[-(1-5\mu)S^3 - (1+3\mu)S^2 + \frac{2}{3}(1-\mu)S + \frac{8}{27}(1+\mu)\right] \tag{3-12}$$

The moment at the centroid of the triangle is

$$M_x = M_y = \frac{qa^2}{54}(1+\mu) \tag{3 - 13}$$

Since the magnitude and position of the maximum moment is a function of μ, moments for various μ and S have been computed and are plotted in Graph 3 - 1.

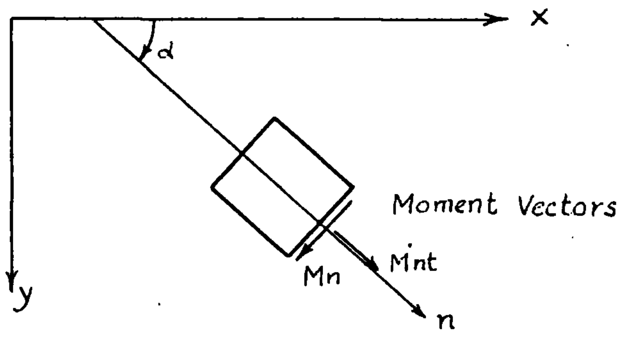

Fig 3 - 6

The moments on any element of area in the plate as shown in Figure 3 - 6 are given by

$$\left.\begin{aligned} M_n &= M_x \cos^2\alpha + M_y \sin^2\alpha - 2M_{xy}\sin\alpha\cos\alpha \\ &\text{and} \\ M_{nt} &= M_{xy}(\cos^2\alpha - \sin^2\alpha) + (M_x - M_y)\sin\alpha\cos\alpha \end{aligned}\right\} \tag{3 - 14}$$

where α is the angle between the x and n axes. The maximum value of Mn occurs at y = 0 and $\alpha = 90^{\circ}$ and is therefore equal to the maximum value of My plotted in

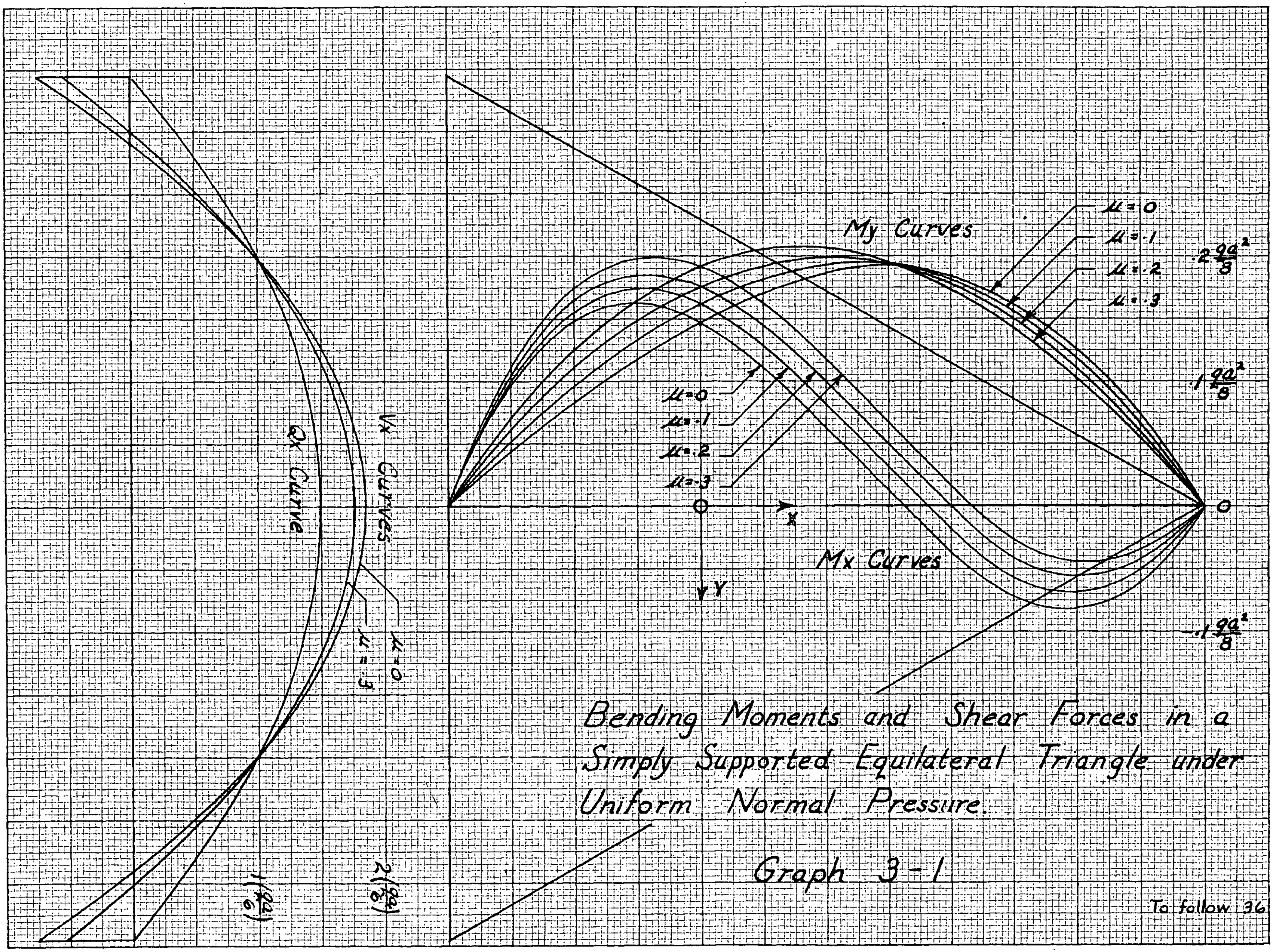

Bending Moments and Shear Forces in a Simply Supported Equilateral Triangle under Uniform Normal Pressure.

Graph 3-1

To follow 36

Graph 3 - 1. The absolute maximum value of Mnt occurs at y = 0, x = .405a and $\alpha = 45^{\circ}$ and is equal to

$$Mnt_{max} = \pm .234 \frac{qa^2 (1-\mu)}{16} \qquad (3 - 15)$$

The corresponding moment on this plane is from Equation 3 - 14

$$\left. M_n \right]_{\substack{\alpha = 45^{\circ} \\ x = .405a}} = \frac{qa^2}{8}(1+\mu)\left[s^3 - s^2 + \frac{4}{27} \right] = .05\,(1+\mu)\,\frac{qa^2}{8} \qquad (3\text{-}15a)$$

The differential equations for the shear forces as defined in Fig 3 - 5 are

$$Q_x = -D \frac{\partial}{\partial x}\left(\frac{\partial^2 w}{\partial x^2} + \frac{\partial^2 w}{\partial y^2} \right)$$
$$Q_y = -D \frac{\partial}{\partial y}\left(\frac{\partial^2 w}{\partial x^2} + \frac{\partial^2 w}{\partial y^2} \right) \qquad (3 - 16)$$

Therefore

$$Q_x = -\frac{q}{4a}\left[-3x^2 + 2ax + 3y^2 \right] \qquad (3 - 17)$$

and

$$Q_y = -\frac{qy}{2a}\left[3x + a \right] \qquad (3 - 18)$$

The shear force along the edge $x = -\frac{a}{3}$ is

$$Q_x = -\frac{3q}{4a}\left[y^2 - \frac{a^2}{3} \right] \qquad (3 - 19)$$

and is identical to the shear force on the other two sides by symmetry. The shear curve is shown also in Graph 3 - 1. The maximum shear on the edge, at y = 0, is also the maximum shear force in the plate with a value.

$$Q_{x_{max}} = Q_{n_{max}} = \frac{qa}{4} \tag{3 - 20}$$

The average shear stress along the edge of the triangle, obtained by dividing the total load on the plate by the perimeter is

$$Q_{x_{ave}} = \frac{qa}{6} \tag{3 - 21}$$

Therefore (3 - 22)

$$Q_{x_{max}} = \frac{3}{2}\ Q_{ave.}$$

The distribution of reactive forces along the edge of a plate is not usually the same as the distribution of shear forces Q. This is because the twisting moments Mxy and Myx contribute an extra load term to the shear Q. The twisting moment Mxy acting on an element of length dy may be replaced, using Saint Venant's principle, by two vertical forces Mxy, dy apart, as shown in Figure 3 - 7.

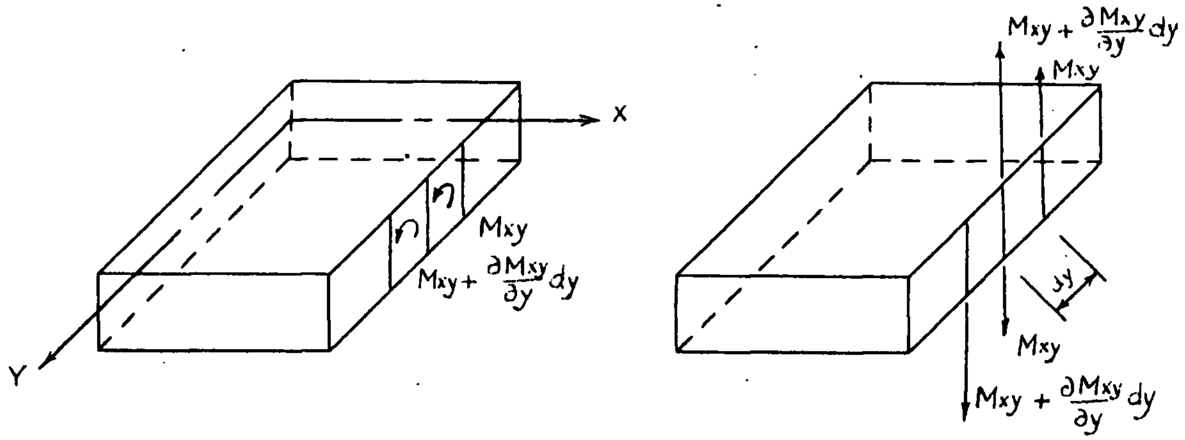

Fig 3 - 7

Summing the forces in the z direction show that the distribution of the twisting moments is statically equivalent to a distribution of shearing forces of $-\frac{\partial M_{xy}}{\partial y}$ per unit length. Therefore the reactive force is

$$V_x = Q_x - \frac{\partial M_{xy}}{\partial y} \tag{3 - 23}$$

For the equilateral triangle along the edge $x = \frac{a}{3}$,

$$\frac{\partial M_{xy}}{\partial y} = \frac{q(1-\mu)}{16a}(9y^2 - a^2) \tag{3 - 24}$$

Therefore the reactive along this edge is

$$V_x = -\frac{q}{16a}\left[12y^2 - 4a^2 + (1-\mu)(9y^2 - a^2)\right] \tag{3 - 25}$$

This curve is also plotted in Graph 3 - 1 for values of $\mu = 0$ and $\mu = .3$ only. Since the two curves lie close together, intermediate values of μ are easily interpolated.

D. COMBINED STRESSES

1. Isotropic Plate.

Before computing the bending stresses and combining them with the membrane stresses, it is convenient to define the stresses that may occur. In Figure 3 - 8, a lamina of the element of plate is separated and the symbolism and positive directions of the stresses indicated.

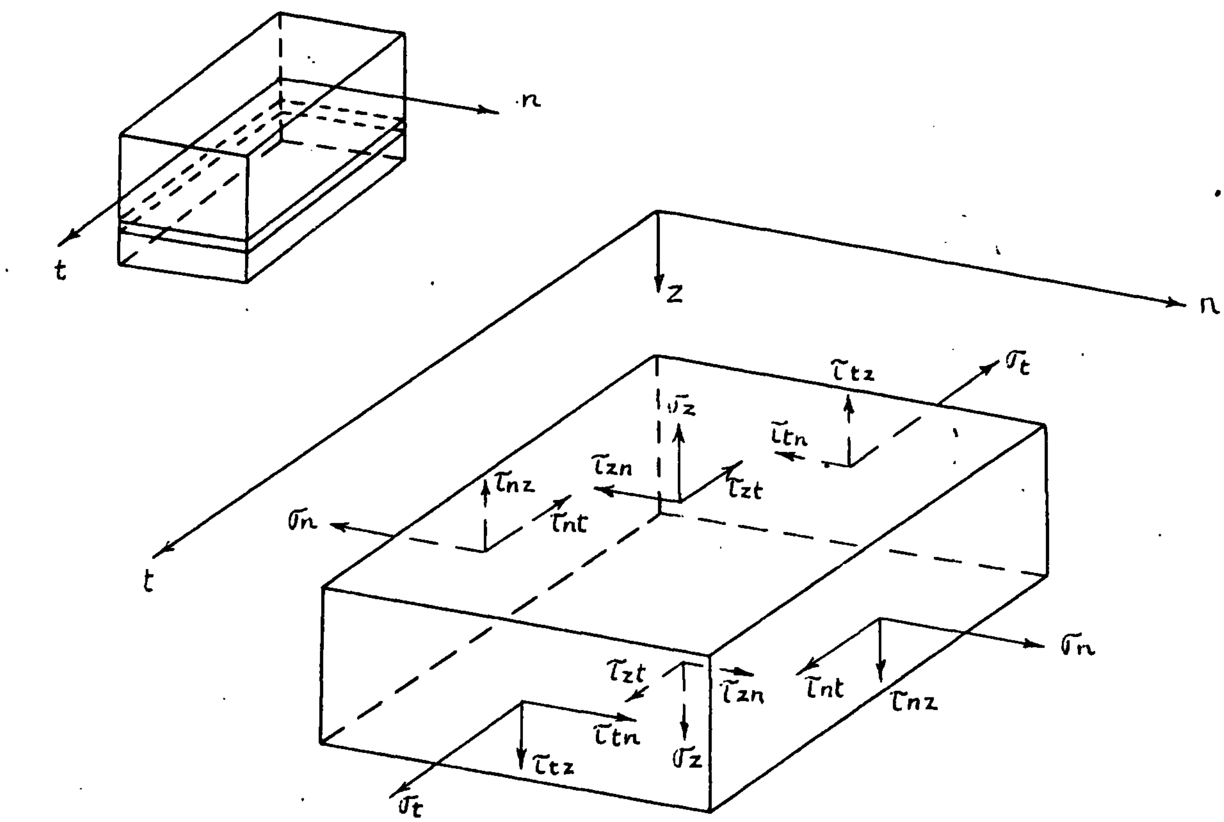

Figure 3 - 8

The normal stresses, denoted by σ_n and σ_t arise from bending moments Mn and Mt and membrane forces Nn and Nt respectively. Shell theory gives the membrane forces in the φ and θ directions only. If the φ, θ co-ordinate axes are not co-incident with the n, t axes, Nn and Nt must be determined from either Mohr's circle of $N\varphi$ and $N\theta$ or the corresponding equations. Remembering that the units for N are lbs per unit length and for M are inch-lbs per unit length, then the stress at the outside fibre is

$$\sigma_n = \frac{N_n}{A} \pm \frac{M_n}{Z} \qquad (3 - 26)$$

where A and Z are the area and section modulus of a unit length respectively. In determining the most severe combination of stress, it should be remembered that the equilateral triangle has three axes of symmetry and the equations previously derived used only one such axis. Also, the position and orientation of the triangle within the shell may vary somewhat.

The membrane shear force Nnt and triangle twisting moment Mnt produce shear stresses $\tau_{nt} = \tau_{tn}$. Shear stresses from Nnt are uniformly distributed across the thickness of the plate. Shear stresses from Mnt are distributed linearly, increasing from zero at the middle plane to a maximum at the outside fibre. Therefore the shear stress at the outside fibre is

$$\tau_{nt} = \frac{N_{nt}}{A} \mp M_{nt} \frac{6}{h^2} \qquad (3 - 27)$$

The shear forces Qn and Qt produce shear stresses $\tau_{nz} = \tau_{zn}$ and $\tau_{tz} = \tau_{zt}$ and do not combine with any stresses produced from shell action. These stresses are distributed parabolically across the plate with the largest stress at the middle plane. Therefore at the middle plane

$$\tau_{nz} = \frac{3}{2} \frac{Q_n}{h} \qquad (3 - 28)$$

The maximum shear stress in the plate is, from Equation 3 - 20,

$$\tau_{nz_{max}} = \tau_{xz_{max}} = \frac{3}{2} \frac{Q_{x\,max}}{h} = \frac{3}{8} \frac{qa}{h} \qquad (3 - 29)$$

2. Plywood.

The equations previously derived are based on an isotropic material. Plywood, however, is not isotropic and the stress equations must be suitably modified. Since two dimensional stress is not usually encountered in the design of more common plywood structures, a brief discussion is included here.

The strength properties of an element of plywood vary with the orientation of the element with respect to the face grain. However, in computing the allowable forces, the element is always considered as oriented so that the n and t axes are parallel and perpendicular to the face grain respectively. Therefore the forces acting on an element are resolved into components giving normal and shear forces as shown in Figure 3 - 9. Then the forces must be such that[5]

$$\left(\frac{f_n}{F_n}\right)^2 + \left(\frac{f_t}{F_t}\right)^2 + \left(\frac{f_{nt}}{F_{nt}}\right)^2 \leq 1 \qquad (3 - 30)$$

where denotes the actual forces acting and F denotes the permissable

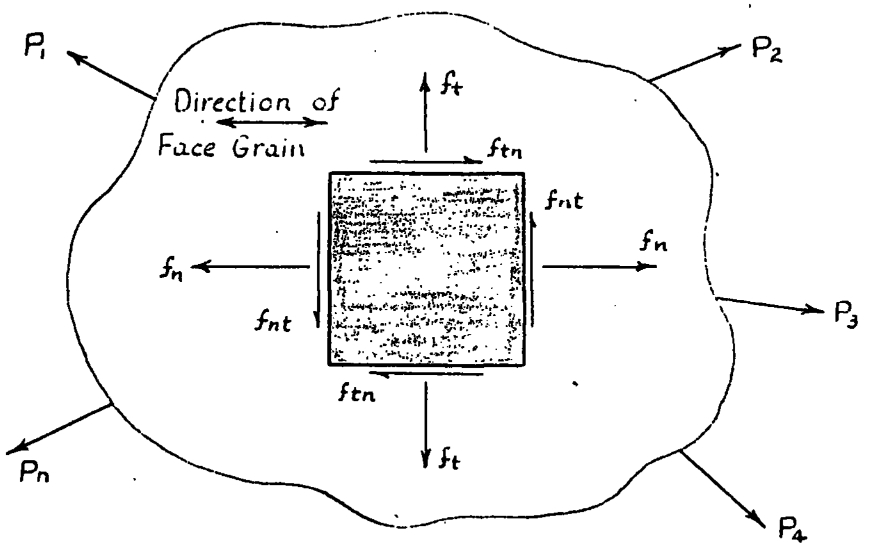

Fig. 3 - 9

[5] Airforce - Navy - Civil Aviation Committee, A.N.C. Handbook on the Design of Wood Aircraft Structures, U.S. Dept. of Agriculture, 1942, P.38

force in that direction if no other forces are acting.

In the determination of normal stress, only those plies with their grain parallel to the applied force are considered as acting. The areas, section moduli and moments of inertia parallel and perpendicular to the face grain for a one foot wide strip are tabulated in Table 1 of the Douglas Fir Plywood Technical Handbook. Denote these values by An, At, Zn, Zt, In and It respectively. Then the combined normal stresses at the outside fibre capable of resisting stress are

$$\left.\begin{aligned} \sigma_n &= \frac{N_n}{A_n} \pm \frac{M_n}{Z_n} \\ &\text{and} \\ \sigma_t &= \frac{N_t}{A_t} \pm \frac{M_t}{Z_t} \end{aligned}\right\} \qquad (3 - 31)$$

The shear stress $\tau_{nt} = \tau_{tn}$ is called "shear through the thickness" in the Douglas Fir Plywood Technical Handbook. In computing this shear stress, the whole cross sectional area is considered as acting. Therefore the equation

$$\tau_{nt} = \frac{N_{nt}}{A} \mp M_{nt}\frac{6}{h^2} \qquad (3 - 27)$$

derived for an isotropic plate may be used.

The values of σ_n, σ_t and τ_{nt} for a point (x, y) are substituted directly into Equation 3 - 30. The allowable stresses in the denominator of this Equation may be obtained from Table 3 of the Douglas Fir Plywood Technical Handbook. The worst stress condition occurs where the left hand side of Equation 3 - 30 is a maximum. This maximum value depends on the co-ordinates of the point, the orientation of the face grain and the position and orientation of the triangle in the shell. Therefore it is not feasible to determine where the maximum occurs other than by a trial and error process. It is recommended here to determine the maximum stresses in the triangle from lateral loads only and then combine them with the membrane stresses in the most severe possible way since it is almost certain that one triangle will be oriented such that this condition applies.

The shear stresses $\tau_{nz} = \tau_{zn}$ and $\tau_{tz} = \tau_{zt}$ produce rolling shear in plywood. The distribution of shear stress is irregular because only those plies parallel to the shear stress act. The shear stresses are given by

$$\tau_{zn} = \frac{Q_n \, S_n}{I_n \, W}$$

and

$$\tau_{zt} = \frac{Q_t \, S_t}{I_t \, W} \qquad . \quad (3 - 32)$$

where Sn and St are the first moments of area of those plies parallel to the n and t axes respectively outside the plane considered. The symbol W denotes the width of the section and the symbols Qn, Qt, In and It are as previously defined. First moments of area are not tabulated in the Douglas Fir Plywood Technical Handbook and so must be computed from the tabulated thicknesses of the plies. The distribution of rolling shear is indicated qualitatively in Figure 3 - 10 for both the n and t directions of a typical section. The shear stress is constant across a perpendicular ply and is distributed parabolically across a parallel ply. Therefore the maximum rolling shear for both the n and t directions may be evaluated at the glue line of the innermost ply. Though the shear stress at the neutral axis for either the n or the t directions is numerically greater, it is not rolling shear but horizontal shear. Since the allowable horizontal shear stress is greater than the allowable rolling shear stress, rolling shear remains the critical stress.

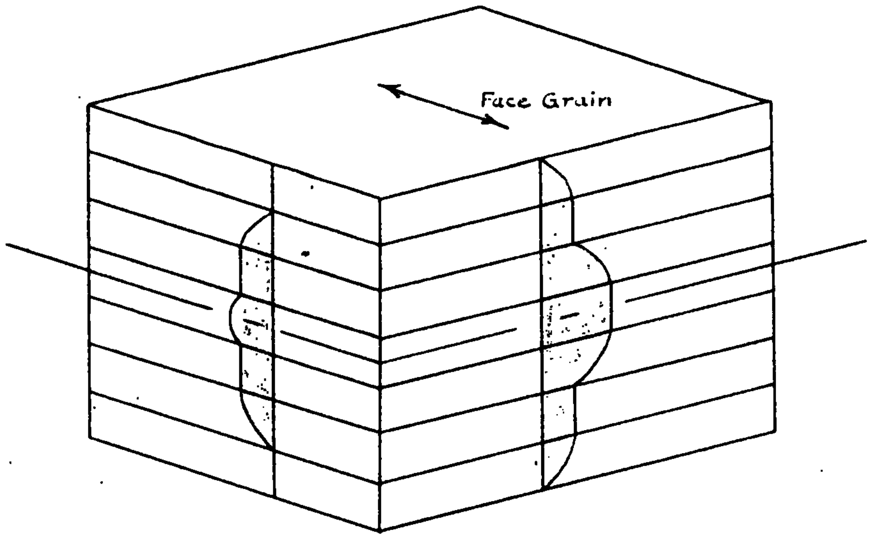

Fig. 3 - 10

E. BUCKLING OF A TRIANGLE

The differential equation for a buckled plate is[6]

$$\frac{\partial^4 w}{\partial x^4} + 2\frac{\partial^4 w}{\partial x^2 \partial y^2} + \frac{\partial^4 w}{\partial y^4} = \frac{1}{D}\left(N_x \frac{\partial^2 w}{\partial x^2} + N_y \frac{\partial^2 w}{\partial y^2} + 2N_{xy}\frac{\partial^2 w}{\partial x \partial y}\right) \quad (3 - 33)$$

where Nx, Ny and Nxy are forces per unit length in the plane of the plate. A lower critical stress is obtained if Nx and Ny are both compressive since tension forces by either Nx or Ny tend to stabilize the plate. In the most severe case, Nx = Ny and Mohrs circle becomes a point so that Nxy = 0/ The differential equation then reduces to

$$\frac{\partial^4 w}{\partial x^4} + 2\frac{\partial^4 w}{\partial x^2 \partial y^2} + \frac{\partial^4 w}{\partial y^4} = \frac{N_x}{D}\left(\frac{\partial^2 w}{\partial x^2} + \frac{\partial^2 w}{\partial y^2}\right) \quad (3 - 34)$$

6 S. Timoshenko, Theory of Elastic Stability, New York, McGraw-Hill, 1936, p. 324

or writing in shorthand notation

$$\nabla^4 w = \frac{N_x}{D} \nabla^2 w \tag{3 - 35}$$

For an exact solution, some function for the deflection w must be obtained which satisfies not only the buckling equation but also the boundary conditions for a simply supported plate. The method of solution closely parallels the solution for bending of an equilateral triangle. However in this case, the expression for w is more complicated and an exact solution does not appear to be feasible.

A solution may be obtained, however, by using finite difference equations. The plate is divided by a grid or network of lines and $\nabla^4 W$ and $\nabla^2 W$ written for each point of intersection of the net. Substituting these expressions into Equation 3 - 34 gives one equation for each point on the plate. The resulting equations are then solved simultaneously for Nx. The degree of accuracy obtained depends on the number of points taken or the finess of the grid interval.

A triangular net is particularly suitable for obtaining a solution to the buckling problem of an equilateral triangle since the net lines are parallel to the edges of the triangle and the boundary conditions are easy to satisfy. Since triangular nets are not in such common use as rectangular nets, a brief explanation is included here.

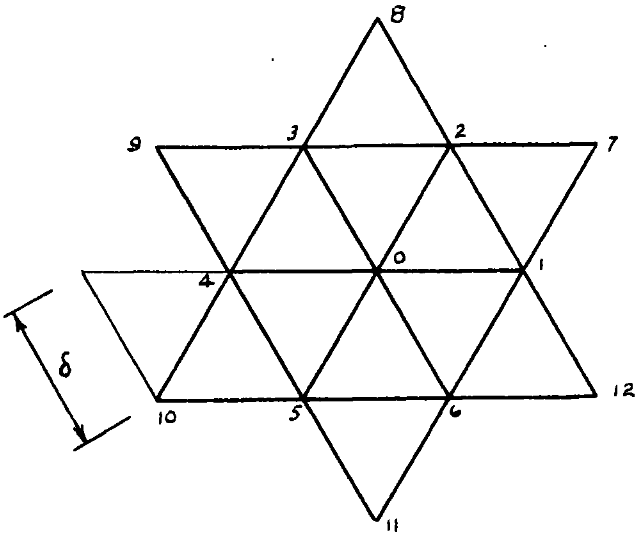

Fig 3 - 11

TRIANGULAR NET

Referring to Figure 3 - 8, let

$$\Sigma w_1 = w_1 + w_2 + w_3 + w_4 + w_5 + w_6$$

and

$$\Sigma w_7 = w_7 + w_8 + w_9 + w_{10} + w_{11} + w_{12}$$

It can be proved that [7]

$$\left.\begin{aligned} \frac{9\delta^4}{16}\left(\nabla^4 w\right)_0 &= 12\, w_0 + \Sigma w_7 - 3\,\Sigma w_1 \\ \text{and} \qquad 9\,\delta^2\left(\nabla^2 w\right)_0 &= 9\,\Sigma w_1 - \Sigma w_7 - 48\, w_0 \end{aligned}\right\} \qquad (3 - 36)$$

Dividing the side of an equilateral triangle into seven equal parts with a triangular net gives fifteen points on the triangle as shown in Figure 3 - 12

[7] Allen, D.N., Relaxation Methods, New York, McGraw-Hill, 1954, p. 146

By symmetry though, there are only four different points.

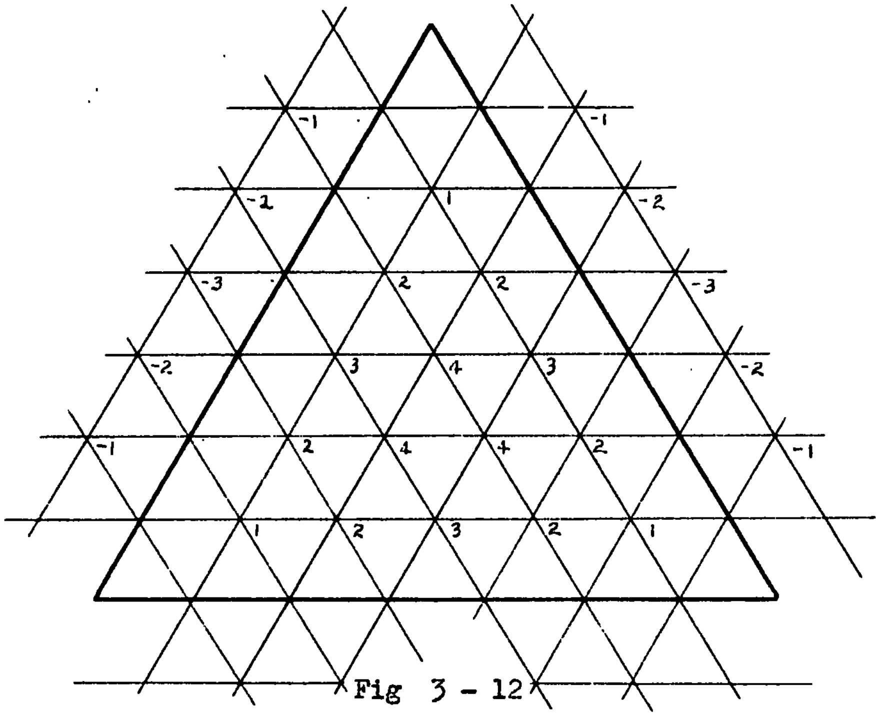

Fig 3 - 12

Writing the expressions for $(\nabla^4 W)_n$, $(\nabla^2 W)_n$, and collecting terms we obtain:

$$\left.\begin{aligned}
9\,\frac{\delta^4}{16}\,(\nabla^4 w)_1 &= 10\,w_1 - 6\,w_2 + w_4 \\
9\,\frac{\delta^4}{16}\,(\nabla^4 w)_2 &= -3\,w_1 + 8\,w_2 - 2\,w_3 - 2\,w_4 \\
9\,\frac{\delta^4}{16}\,(\nabla^4 w)_3 &= -4\,w_2 + 11\,w_3 - 5\,w_4 \\
9\,\frac{\delta^4}{16}\,(\nabla^4 w)_4 &= w_1 - 4\,w_2 - 5\,w_3 + 6\,w_4
\end{aligned}\right\} \qquad (3 - 37)$$

$$\left.\begin{aligned}
9\,\delta^2\,(\nabla^2 w)_1 &= -46\,w_1 + 18\,w_2 - w_4 \\
9\,\delta^2\,(\nabla^2 w)_2 &= 9\,w_1 - 38\,w_2 + 8\,w_3 + 8\,w_4 \\
9\,\delta^2\,(\nabla^2 w)_3 &= +16\,w_2 - 47\,w_3 + 17\,w_4 \\
9\,\delta^2\,(\nabla^2 w)_4 &= -w_1 + 16\,w_2 + 17\,w_3 - 30\,w_4
\end{aligned}\right\} \qquad (3 - 38)$$

Before substituting into Equation 3 - 34, it must be modified to

$$\frac{9\delta^4}{16}(\nabla^4 w)_n = \left[\frac{N_x}{D}\frac{\delta^2}{16}\right] 9\,\delta^2 (\nabla^2 w)_n \tag{3 - 39}$$

or

$$\frac{9\delta^4}{16}(\nabla^4 w)_n = \beta \quad 9\,\delta^2 (\nabla^2 w)_n \tag{3 - 40}$$

where

$$\beta = \frac{N_x\ \delta^2}{16\ D} \tag{3 - 41}$$

Substituting Equations (3 - 37) and 3 - 38) into Equation (3 - 40) and collecting terms give

$$\begin{aligned}
(10 + 46\beta)w_1 - (6 + 18\beta)w_2 + 0 \qquad\qquad + (1 + \beta)w_4 &= 0\\
-(3 + 9\beta)w_1 + (8 + 38\beta)w_2 - (2 + 8\beta)w_3 - (2 + 8\beta)w_4 &= 0\\
0 \quad - (4 + 16\beta)w_2 + (11 + 47\beta)w_3 - (5 + 17\beta)w_4 &= 0\\
(1 + \beta)w_1 - (4 + 16\beta)w_2 - (5 + 17\beta)w_3 + (6 + 30\beta)w_4 &= 0
\end{aligned}$$

One solution of the four equations is $W = 0$. However this is not a buckled shape and is therefore a trivial solution. The only non zero solution is for the determinant of the coefficients to vanish. Therefore the solution of the four equations is obtained from

$$\begin{vmatrix}
(10 + 46\beta) & -(6 + 18\beta) & 0 & (1 + \beta)\\
-(3 + 9\beta) & (8 + 38\beta) & -(2 + 8\beta) & -(2 + 8\beta)\\
0 & -(4 + 16\beta) & (11 + 47\beta) & -(5 + 17\beta)\\
(1 + \beta) & -(4 + 16\beta) & -(5 + 17\beta) & (6 + 30\beta)
\end{vmatrix} = 0$$

which yields

$$1,141,114\beta^4 + 820,358\beta^3 + 207,858\beta^2 + 21,266\beta + 686 = 0$$

The real root of this equation giving the smallest compressive load is $\beta = -.059$

Substituting into Equation 3 - 41 gives

$$\frac{N_x\,\delta^2}{16\,D} = -.059$$

Replacing by its value $b/7$, multiplying the numerator and denominator by π^2 and arranging terms, the critical load is

$$(N_x)_{cr} = -4.66\,\frac{\pi^2 D}{b^2} \qquad (3 - 42)$$

where b is the length of the side of the triangle. The form of Equation 3 - 42 is now the same as the form of the buckling equation for a column since $D \cong EI$. The minus sign in Equation 3 - 42 indicates that the critical force is compressive as was suggested in the previous discussion of the buckling problem.

A similar procedure using a different number of points on the triangle gives various values of K in the equation

$$(N_x)_{cr} = K\,\frac{\pi^2 D}{b^2} \qquad (3 - 43)$$

Plotting a graph of K versus the total number of points on the triangle gives the curve shown in Figure 3 - 13. Since the curve is asymptotic to K = - 4.75, the equation for buckling of a simply

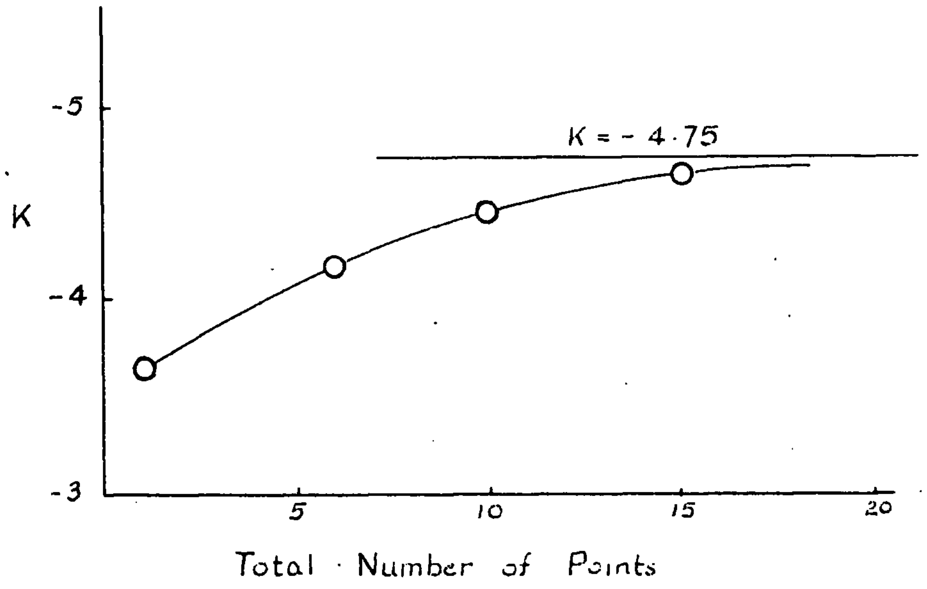

Fig 3 - 13

supported equilateral triangle is

$$(N_x) = -\ 4.75\ \frac{\pi^2 D}{b^2} \qquad (3-44)$$

Not all the triangles comprising a geodesic shell are equilateral so that the coefficient K must be determined for other shapes as well. For convenience, only isosceles triangles are considered so that the shape of a triangle is determined by the two parameters, b and γ , as defined in Figure 3 - 14. For the same

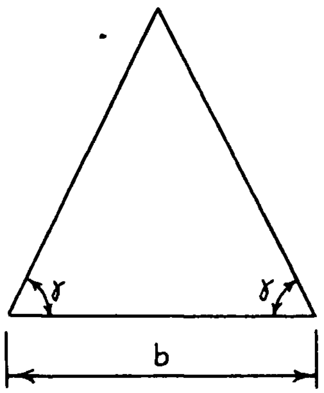

Fig 3 - 14

stress conditions, $N_x = N_y$, Timoshenko[8] gives the buckling load on a simply supported isosceles right triangle, $\gamma = 45^\circ$, as

$$(N_x) = -\ 10\ \frac{\pi^2 D}{b^2}$$

While all the triangles encountered in a geodesic shell lie within the range

$$45^\circ < \gamma \leq 60^\circ$$

it is not safe to assume a linear variation of K. Since boundary conditions are

[8] S. Timoshenko, Theory of Plates and Shells, New York, McGraw-Hill, 1940, p 311

hard to satisfy without convenient co-ordinates, it is impractical to investigate cases within the range

$$45^\circ < \gamma < 60^\circ$$

However, investigation of a few cases outside this range makes it possible to draw the curve of K and γ with sufficient accuracy.

For the case $\gamma = 30^\circ$, using a triangular net and writing four finite difference equations again, the critical load is

$$(Nx) = -32 \frac{\pi^2 D}{b^2} \qquad (3 - 45)$$

The buckling load for a simply supported rectangular plate when $Nx = Ny$ is [9]

$$(Nx) = -\frac{\pi^2 D}{b^2}\left(1 + \frac{b^2}{a^2}\right) \qquad (3 - 46)$$

when a and b are the lengths of the sides. This formula may be used to investigate the limiting conditions of $\gamma = 0^\circ$ and $\gamma = 90^\circ$. As $\gamma \rightarrow 90^\circ$, $a \rightarrow \infty$ and

$$(Nx) = -\frac{\pi^2 D}{b^2} \qquad (3 - 47)$$

As $\gamma \rightarrow 0^\circ$, $a \rightarrow 0$ and

$$(Nx) \rightarrow -\infty$$

Graph 3 - 2 shows the result of plotting K as ordinates and γ as abscissae.

[9] Timoshenko, S., Elastic Stability
New York, McGraw-Hill, 1936, p 333

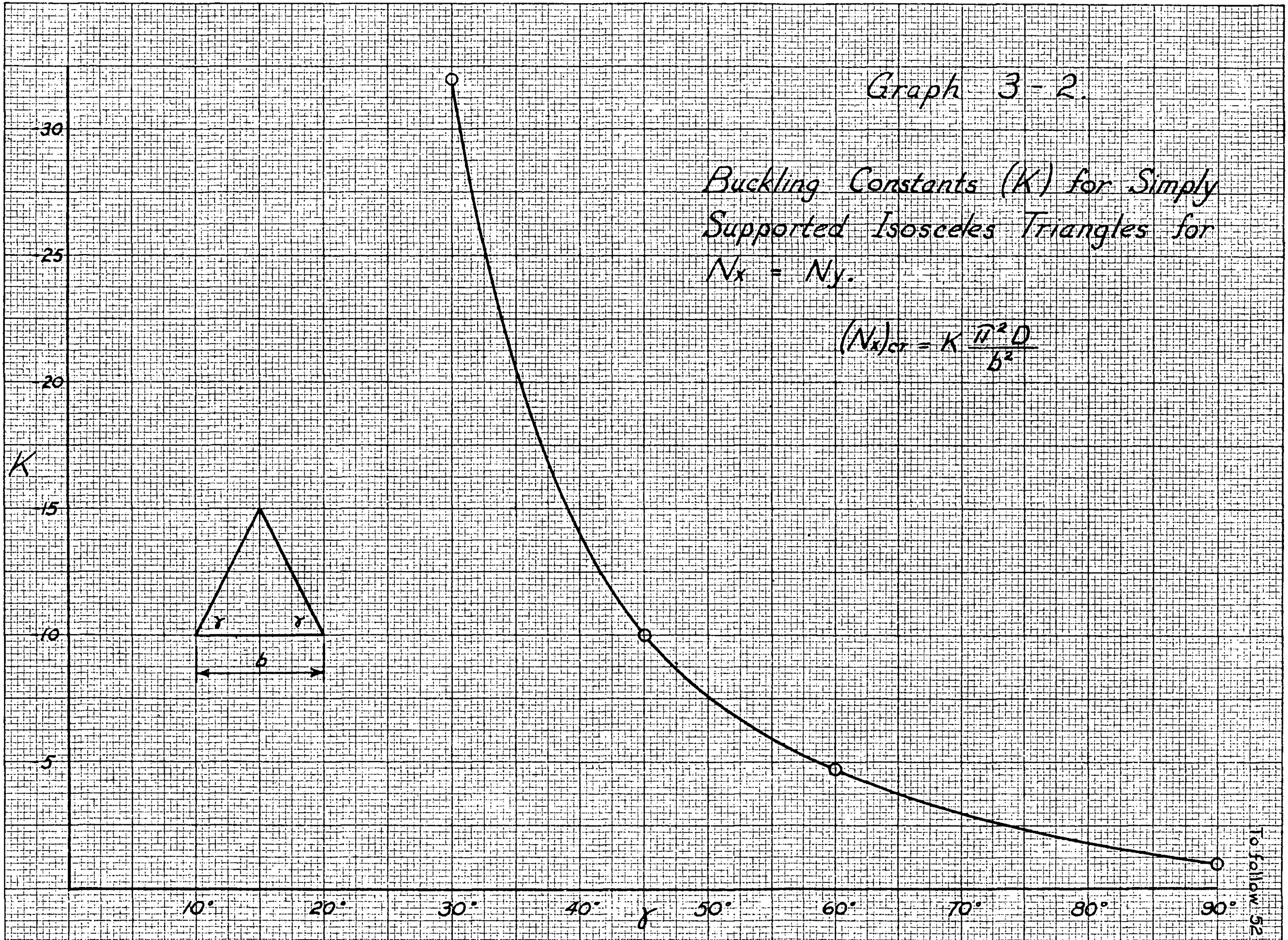

Graph 3 - 2.
Buckling Constants (K) for Simply Supported Isosceles Triangles for $N_x = N_y$.
$(N_x)_{cr} = K \frac{\pi^2 D}{b^2}$
K
30
25
20
15
10
5
γ
γ
b
10°
20°
30°
40°
γ
50°
60°
70°
80°
90°

To follow 52

Some of the triangles encountered in the dome may be scalene instead of isosceles. The change from an isosceles triangle is not great. Therefore substituting with care an isosceles triangle for a scalene triangle gives a good value of the critical load.

Despite the fact that there is some rigidity at the boundary, assuming simply supported plates is not unreasonable because one plate may buckle in and the other out as shown in Figure 3 - 15. Therefore the joint rigidity does little to prevent buckling.

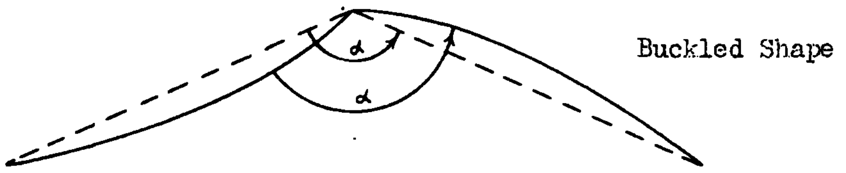

Fig 3 - 15

The flexural rigidity of a plate, appearing in the buckling equation, is

$$D = \frac{Eh^3}{12(1-\mu^2)} \tag{3 - 48}$$

where h is the thickness of the plate. Letting $\mu = o$, the flexural rigidity becomes

$$D = \frac{Eh^3}{12} = E\,I \tag{3 - 49}$$

since $h^3/12$ is the moment of inertia of a unit width of plate. While Equation 3 - 48 is applicable for isotropic plates, Equation 3 - 49 is better used for plywood. Using $E = 1.8\ (10^6)$ and determining the average I from Table 1 of the Douglas Fir Plywood Technical Handbook, an average flexural rigidity is easily obtained.

F. BUCKLING OF THE SHELL

Since the analysis of the critical stress of thin shells is a fairly complex problem no attempt will be made here to present the lengthy differential and energy equations. Instead, the general attack and final results will be discussed and the latter put into a form useful for the design of geodesic shells. The latter part of this section is devoted to the application of these equations to plywood since the original derivations assume an isotropic plate.

For a spherical shell under a uniform external pressure p, Mohr's circle of stress is a point and

$$\sigma = \frac{p\rho}{Eh} \tag{3 - 50}$$

For this stress condition, the so-called classical theory of buckling of thin shells gives a critical stress of

$$\sigma_{cr} = \frac{1}{\sqrt{3(1-\mu^2)}} \; \frac{Eh}{\rho} \tag{3 - 51}$$

This classical theory assumed small deflections and a buckled surface dependant only on φ and independant of θ. However experimental results give a buckling stress three times lower than the classical theory. A similar discrepancy also exists between the theoretical and experimental analysis of cylindrical shells under axial load. Many well known scientists attempted to explain this discrepancy by considering the effect of end conditions and initial deviations from the true shape. Their results indicated a plastic failure of the material which is not substantiated experimentally since releasing the load removes the buckling waves. Also buckling occurs suddenly not gradually as is required for a plastic failure.

The real reason for the discrepancy was later explained by T. von Karman and Hsue - Shen Tsien[10]. These authors pointed out that the classical theory assumed small deflections and thus obtained a linear differential equation determining the equilibrium position of the shell whereas actually large deflections occur and the differential equation is non linear. They also observed that the buckled wave form was not as predicted by the classical theory but formed a small dimple subtended by a solid angle of approximately sixteen degrees. Therefore they confined their analysis to one dimple indicated in Fig 3 - 16.

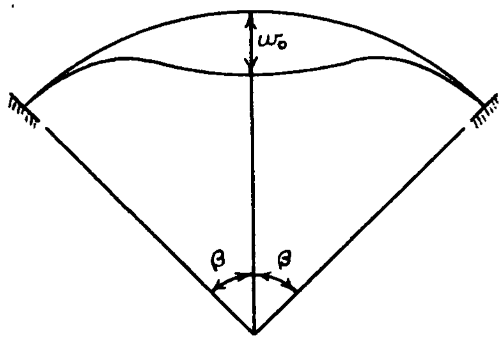

Fig 3 - 16

They assumed that : the solid angle 2β is small, the deflection is rotationally symmetric, the deflection of any element of the shell is parallel to the axis of rotational symmetry and that Poisson's ratio is zero. They then obtained an energy equation for the extensional energy before and after buckling, the bending energy, and the work done by the external pressure during buckling.

[10] Th. von Karman and Hsue-Shen Tsien, "The Buckling of Spherical Shells by External Pressure", Journal of the Aeronautical Sciences, vol. 7 (December 1939). pp. 43 -50

Minimizing this expression to obtain the lowest energy condition gave an expression

$$\frac{\sigma \rho}{Eh} = f\left(\beta^2 \frac{\rho}{h}, \frac{w_o}{h}\right) \tag{3 - 52}$$

where w_o is the maximum deflection of the dimple. Then assigning a value to either $\beta^2 \frac{\rho}{h}$ or $\frac{w_o}{h}$, a plot of the remaining two dimensionless quantities is obtained. Such a plot is shown in Graph 3 - 3 . From this graph the minimum value is

$$\left(\frac{\sigma \rho}{Eh}\right)_{min} = .183 \tag{3 - 53}$$

This value of the critical stress is approximately three times lower than the classical theory and corresponds very closely with experimental results. That large deflections occur is shown by the fact that for the minimum value of $\frac{\sigma \rho}{Eh}$, $\frac{w_o}{h} = 10$ whereas small deflection theory requires that $\frac{w}{h} \leq \frac{1}{2}$.

Since the shape of a geodesic shell so closely conforms to the shape of a true sphere it seems reasonable to apply Karman and Tsien's results to shells of this type. Since the shape of the geodesic shell is not exactly similar, the work done by the external pressure is less than in the Karman and Tsien analysis. However the bending energy of the joining battens is not included so that any error tends to balance out. The magnitude of the solid angle subtending the buckled dimple is approximately sixteen degrees. This suggests that in a geodesic shell the apex of a group of five or six triangles would buckle inwards. Buckling commences at least as a type of local instability since the dimples are small and were analyzed as a single unit. Therefore even though a shell under external pressure is an unusual load for a roof as a whole, it is very nearly the case for

Critical Stresses in a Spherical Shell under Uniform Normal External Pressure.

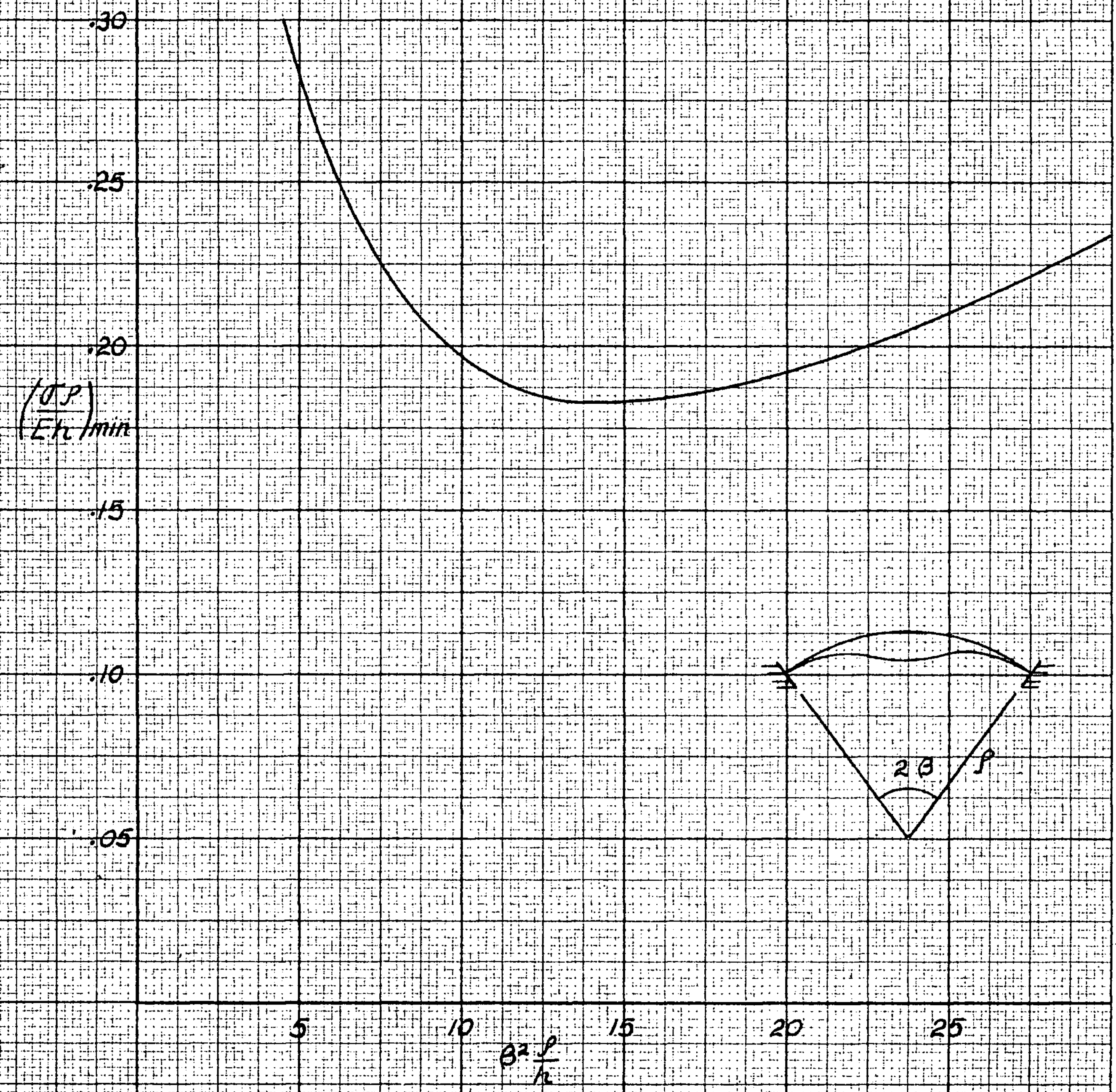

Graph 3-3

the section near the crown. At the crown, dead and live loads produce equal membrane stresses in all directions and the load is nearly normal to the surface. Therefore the loading at the crown is the same as for a spherical shell under external pressure and the energy expressions of Karman and Tsien are justified for this section of the roof. At other sections of the roof the loading is less severe with regard to buckling since the external load is less and the membrane stresses are smaller.

Instability may occur in a geodesic shell in one of two ways. A group of triangles may buckle or an individual triangle may buckle. In the first case, as presented in this section, $\left(\frac{\sigma \rho}{Eh}\right)$ is a constant. In the second case, discussed in the previous section, the buckling force is

$$N_{cr} = K \frac{\pi^2 D}{b^2} \tag{3 - 43}$$

where b is defined as the base of the triangle and K is a constant depending on the shape of the triangle. However the base is a function of the radius. Represent this function by λ which is tabulated in Chapter II. For the case $\mu = 0$, $D = \frac{Eh^3}{12}$ and the critical force is

$$N_{cr} = K \pi^2 \frac{Eh^3}{12 \lambda^2 \rho^2} \tag{3 - 54}$$

or

$$\frac{\sigma \rho}{Eh} = \frac{K \pi^2}{12 \lambda^2} \left(\frac{h}{\rho}\right) \tag{3 - 55}$$

This function is plotted in Graph 3 - 4 for an equilateral triangle and various values of $\frac{\rho}{h}$. Superimposed on this graph is the straight line $\frac{\sigma \rho}{Eh} = .183$, the critical condition for shell buckling. Entering the graph with values of $\frac{\rho}{h}$ and λ determines which type of buckling occurs at the lower stress.

Relation between Buckling of Simply Supported Equilateral Triangles and Spherical Shells under Uniform Normal Pressure.

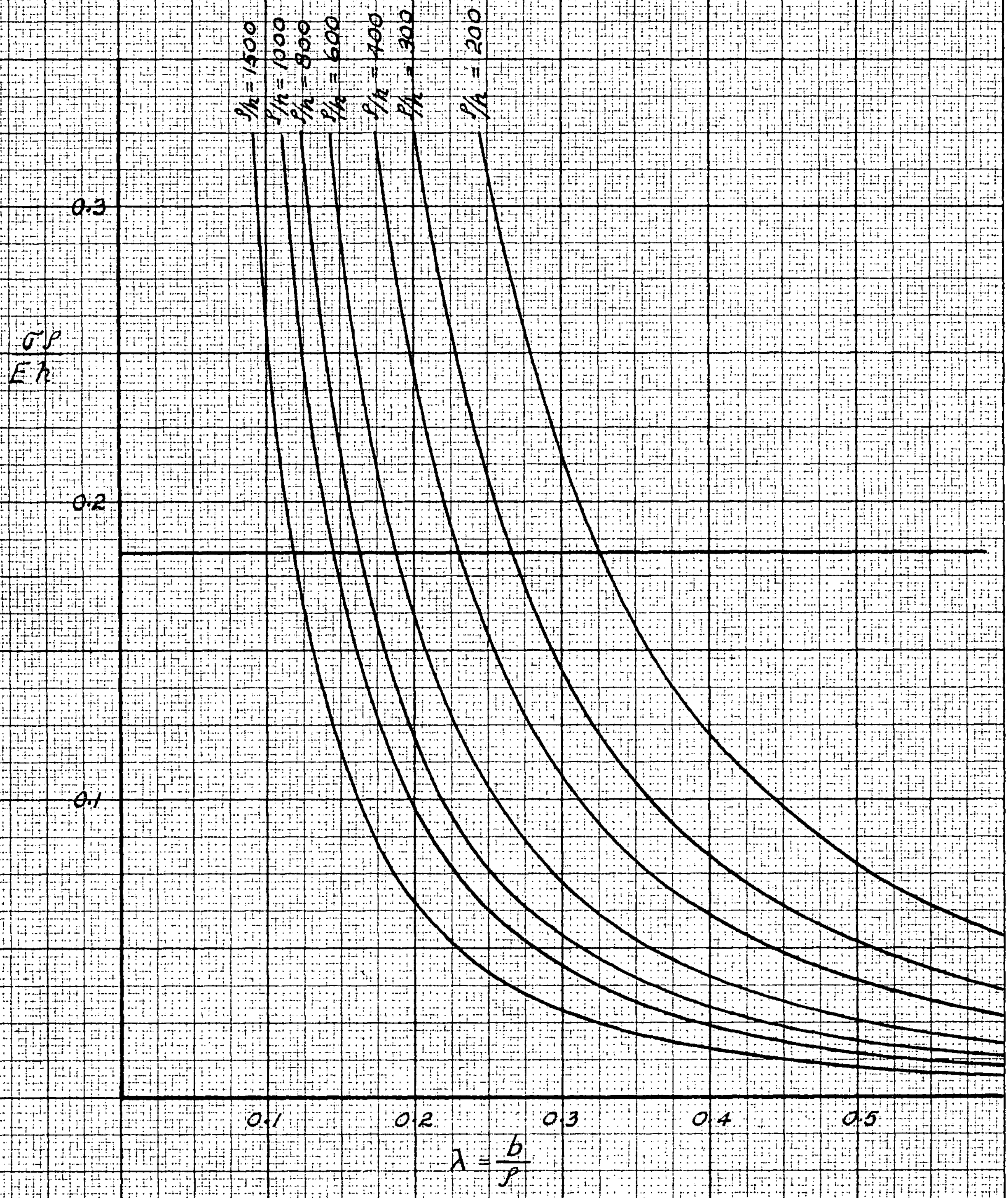

Graph 3-4

For plywood, substituting into the dimensionless quantities $\frac{\sigma \rho}{Eh}$ and $\frac{\rho}{h}$ immediately raises the question of what values to use for E and h. If the full thickness is used then E must be reduced from the parallel to grain value to some smaller average value. This procedure is given in the Wood Handbook.[11.] However there is an easier approach which yields almost identical results. In the previous section the flexural rigidity was modified to

$$\frac{Eh^3}{12(1-\mu^2)} \approx \frac{Eh^3}{12} = E\ I\ ave. \qquad (3 - 49)$$

where Iave is the average of the moments of inertia parallel and perpendicular to the face grain for a unit width. Carrying this approach one step further gives

$$h_{eff} = \sqrt[3]{Iave} \qquad (3 - 56)$$

when Iave is for a one foot width. Equation 3 - 56 defines an effective thickness in inches for substituting into the dimensionless quantities $\frac{\sigma \rho}{Eh}$ and $\frac{\rho}{h}$ used in Graph 3 - 4. When the effective thickness is used, Young's modulus may be taken as $E = 1.8 \times 10^6$ p.s.i. Values of the effective thickness are tabulated in Table 3 - 1. This table illustrates an interesting relation between the effective and nominal thicknesses. Therefore the effective thickness may equally well be taken as

$$h = .79\,h.$$

11 Forest Products Laboratory, Wood Handbook, Washington, U. S. Department of Agriculture, 1955, p.280.

Table 3 - 1

h	$I_{\parallel}$	$I_{\perp}$	I_{ave}	h_{eff}	$\frac{h_{eff}}{h}$
3/8 S	.0435	.00926	.0264	.298	.795
3/8 U	.0427	.00474	.0237	.287	.765
1/2 S	.0730	.0520	.0625	.397	.795
1/2 U	.0961	.0252	.0606	.392	.785
5/8 S	.121	.123	.122	.496	.794
5/8 U	.194	.0353	.1147	.486	.777
3/4 S	.228	.194	.211	.596	.795
3/4 U	.260	.160	.210	.594	.792

CHAPTER IV

EXPERIMENTAL ANALYSIS

A. PRELIMINARY CONSIDERATIONS.

Because of a lack of tabulated functions, the exact analysis was not obtained. The approximate solution developed used smooth shell theory to give the average membrane force on the edge of a triangle but did not give the distribution of these forces. The Fourier analysis for the distribution of the membrane forces also lacked tabulated functions so it was necessary to obtain the distribution experimentally. Therefore the purpose of the model analysis is two-fold. First of all, it should demonstrate the validity of applying the membrane theory of smooth shells to folded plate shells as outlined in Chapter 3. Secondly, it should indicate the distribution of membrane force along the edges of the triangle. It is not the object of the experimental work to ascertain the stress at all points of the dome.

The previous chapter suggested that the distribution of membrane force was, in part, dependent on the dihedral angle formed by two adjacent triangles with the highest stress riser accompanying the largest departure from a dihedral angle of 180°. Excluding the icosahedron as too rough an approximation of a sphere, the next worse case is a sphere composed of 80 triangles. The size of the triangles is governed by the number of points necessary to plot accurately the distribution curve. Electric resistance strain rosettes are approximately two inches square. Therefore to obtain a distribution curve along the edge of a triangle from seven or eight points, the minimum size of triangle must be sixteen to eighteen inches on a side. These criteria outline the geometric limiting conditions of the model.

The three materials considered for making the model were aluminum, plywood and plexiglas. With the equipment available, plywood is the easiest to work with, followed by plexiglas then aluminum. The disadvantages of plywood for model analysis though are important. It is not isotropic with the result that the principal strains are not in the same direction as the principal stresses. In addition, the elastic properties vary uncertainly with a change of moisture content in the plywood. The numerical value of the elastic properties is another prime consideration. Values of Youngs Modulus are approximately:

Aluminum	10×10^{6} lb/ in^{2}	
Wood	1.8×10^{6} lb/ in^{2}	(Parallel to grain)
Plexiglas	0.5×10^{6} lb/ in^{2}	

The comparatively heavy loads required to produce high membrane stresses in a shell are difficult to apply in the laboratory without special loading equipment. But for the same load and cross sectional area, plexiglas gives strains twenty times larger than aluminum. These larger strains are more accurately read on the strain indicator. To obtain the same strain for a given load, aluminum must be 1/20 the thickness of plexiglas. This, however, reduces the buckling load 400 times and aluminum sheet becomes more unstable than plexiglas. Weighing the advantages and disadvantages so far outlined, plexiglas appears the most suitable material for the model.

Plexiglas does have a definite tendency to creep, particularly at the higher stresses. About 85% of the creep occurs in the first few seconds of loading and the remaining 15% over a period of ten to fifteen minutes. However the unit stresses are so low and the time factor so short that creep is not of major importance in this case.

B. DESCRIPTION OF MODEL

After some thought and a few preliminary tests, it was decided to build a five foot diameter hemisphere of forty triangles made from 1/8" plexiglas. This gives ten equilateral triangles 18.54 inches on an edge and thirty isosceles triangles with a base of 18.54" and two sides 16.40 inches. Pictures of the model are included in the photographic supplement. To resemble a dome in actual practise, battens one inch wide and 1/4" maximum depth were used to reinforce the joint. The battens were not connected together and stopped short of the triangle vertices by 1/4". Ordinary CIL cement was used to hold the structure together since laboratory tests showed it to be stronger than other glues tested including a mixture of plexiglas and ethylene chloride. The dome was supported on a heavy ring about three and a half feet above the floor. The ring resisted any horizontal deflection of the base of the shell but was not connected to the shell in a manner to resist rotation of the base of the shell.

After the triangle thickness was measured with a micrometer, thirty eight S R 4 strain rosettes were glued on one isosceles triangle. The position and orientation of the rosettes and the plate thicknesses are given in Figure 4 - 1. The type CR - 1 rosette was used which is made of Iso-elastic wire. In this type of rosette, three strain gages are superimposed one on the other and oriented at forty five degrees to each other.

Iso-elastic rosettes were used because they have a Gage Factor of 3.42 compared to 2.0 for the more common type of rosette made from Constantan wire. If the Gage Factor dial of the Strain Indicator is set at 2.0 when Iso-elastic gages are used, the indicated strain is not the true strain. The true strain is given by

$$\in \text{true} = \in \text{indicated} \times \frac{\text{G.F. dial}}{\text{True G.F.}} \qquad (4 - 1)$$

Thus Iso-elastic gages magnify the true unit strain by 71%. This is particularly advantageous when measuring small strains. The disadvantage to Iso-elastic gages is that they are highly sensitive to temperature changes.

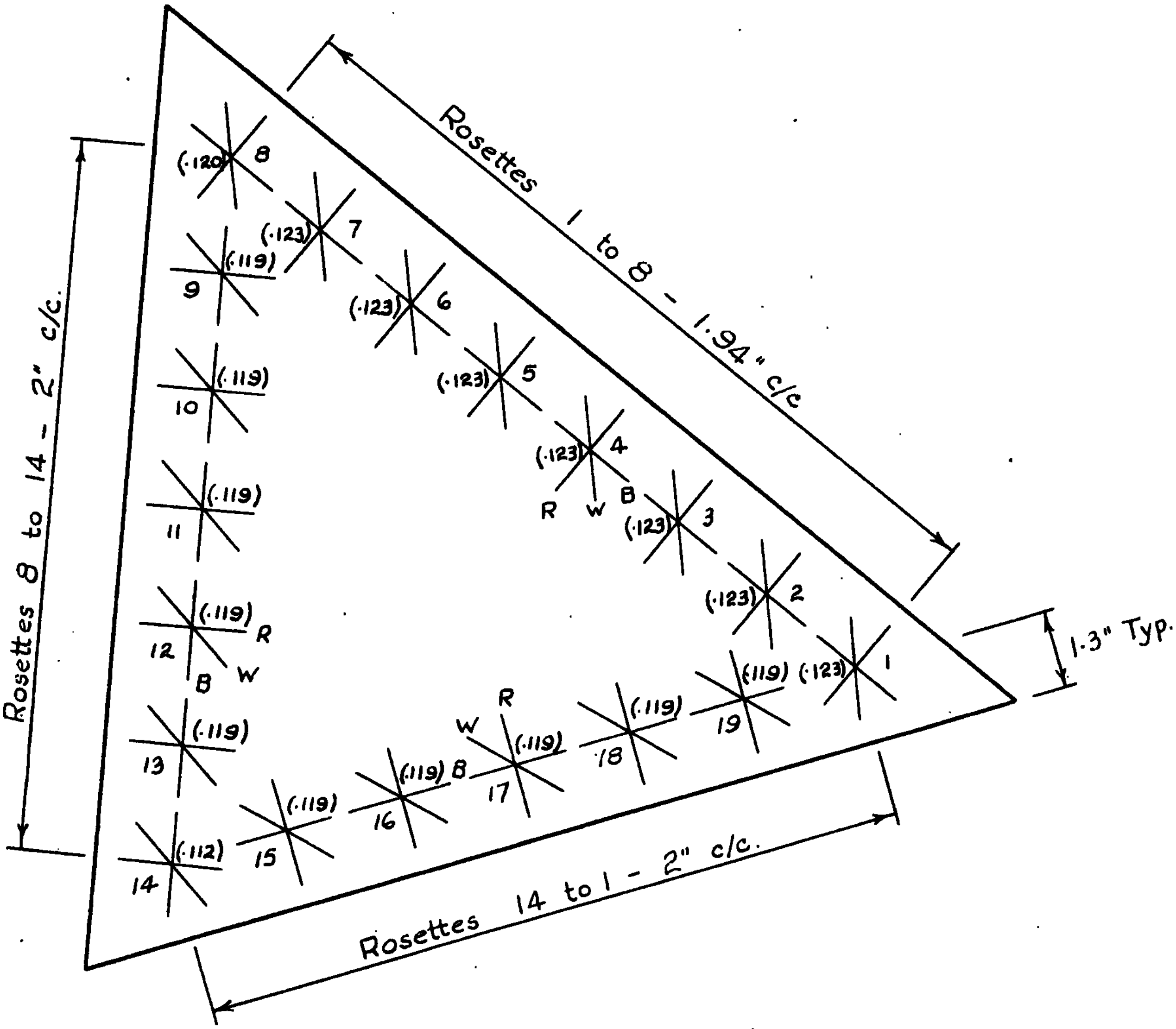

Fig 4 - 1 Placing of Rosettes as viewed from the outside of the shell. Plate thicknesses are in parentheses.

The rosettes were wired with a common ground on each side of the shell. For the other wires, a simple color code facilited differentiating between gages. Red designates all gages normal to the edge of the triangle; white, 45° to the edge and blue, parallel to the edge. The weight of wire was carried by two triangular wooden frames suspended approximately 3/4" above and below the rosettes.

Since there are 114 active wires and two ground wires leading from the shell to the Strain Indicator, a switching unit would be useful. Investigation revealed, however, that this was impractical because the contact resistance of commercial type switches was not constant, giving erroneous strain readings. Good switching units with a near constant contact resistance are very expensive and were therefore beyond reach considering the number required. The only alternative was to connect each wire directly to the Strain Indicator, individually, as required. To separate the maze of wires, they were separated in groups of nine, attached to circular discs, and clearly labelled.

It was noticed with the temperature sensitive gages used that when the circuit was closed, the Wheatstone Bridge did not stay balanced. Visually, the galvanometer needle deflected rapidly at first but gradually slowed as time expired. A permanent balance of the bridge was obtained about five minutes later. This phenomenon was probably due to the heat produced from the electric current passing through the gage resistance. Galvanometer equilibrium would then occur when the strain gage was in thermal equilibrium.

Though temperature compensating gages were used, they are not practically speaking 100% efficient. This slight inefficiency is greatly magnified by the temperature sensitive Iso-elastic gages. Therefore any change of room temperature over the period of testing slightly changes the zero load reading of the gage. In addition, changes of room temperature induce temperature stresses in the model.

These temperature effects are eliminated by the method of loading. One gage is connected to the Strain Indicator and the circuit closed. After the Wheatstone Bridge appeared permanently balanced, loads were applied relatively quickly, taking intermittent readings, up to the maximum load and back again to the zero load. If the Bridge balance was the same at the end of loading as it was at the start, then all temperature effects are nullified and the recorded strains are due only to the applied load.

The loading of the shell was accomplished using one hydraulic jack and an arrangement of beams dividing the total load into six equal parts. One sixth of the load was applied at the top and the remaining five sixths at the five uppermost points formed by the five triangles adjacent to the top. The total load applied to the shell was measured with a proving ring graduated in 1.065 pound divisions. The jack was regulated by levers permitting the operator to control the load and read the Strain Indicator from the same position.

C. ROSETTE ANALYSIS.

After a consistent set of readings, void of temperature effects, were obtained, the values for each side were averaged and the results were plotted. The readings are tabulated in Table 4 - 1 and a typical graph is shown in Figure 4 - 2. In all cases, the results plotted as a straight line.

Table 4-1

Gage		Total Load in Lbs.									
		Side A (outside)					Side B (inside)				
		0	100	200	300	400	0	100	200	300	400
1	R	1299	1375	1458	1540	1621	1356	1368	1381	1394	1409
	W	939	941	942	943	944	1141	1063	983	905	825
	B	1079	1061	1042	1024	1004	1202	1152	1099	1045	991
2	R	1203	1213	1223	1233	1242	1220	1248	1278	1307	1338
	W	1020	978	931	888	843	1068	1078	1088	1099	1110
	B	1928	1898	1864	1831	1799	1183	1173	1163	1152	1141
3	R	1160	1163	1167	1169	1172	1470	1488	1508	1527	1547
	W	1330	1302	1274	1245	1214	1238	1252	1270	1288	1306
	B	1460	1437	1410	1383	1356	1310	1298	1281	1265	1250
4	R	1100	1107	1113	1121	1129	1599	1607	1616	1625	1633
	W	1381	1363	1343	1323	1303	1600	1616	1631	1648	1663
	B	1121	1100	1078	1055	1032	1588	1569	1550	1531	1512
5	R	1303	1315	1328	1341	1355	1338	1336	1332	1330	1328
	W	1511	1499	1479	1462	1447	1328	1332	1339	1341	1348
	B	1440	1420	1400	1380	1359	1259	1240	1221	1201	1180
6	R	1557	1572	1589	1606	1623	1753	1742	1731	1721	1710
	W	959	940	919	898	878	938	923	909	893	878
	B	1212	1193	1172	1151	1129	888	866	842	818	793
7	R	1591	1602	1615	1627	1640	1359	1340	1321	1302	1283
	W	1202	1166	1128	1088	1050	1223	1181	1132	1083	1032
	B	1175	1153	1129	1107	1081	990	960	927	892	858
8	R	1375	1350	1319	1292	1262	1102	1078	1045	1012	978
	W	1395	1321	1239	1163	1083	1935	1856	1761	1671	1578
	B	1602	1570	1537	1500	1461	1878	1860	1842	1823	1802
9	R	1441	1444	1443	1451	1455	1243	1289	1340	1390	1442
	W	1300	1262	1223	1183	1145	1290	1271	1252	1233	1214
	B	1498	1431	1358	1286	1212	948	890	825	761	692
10	R	1889	1890	1890	1891	1891	1259	1298	1340	1381	1425
	W	1227	1192	1158	1125	1091	1528	1519	1512	1504	1497
	B	999	933	868	802	733	1530	1477	1419	1361	1301

Table 4-1 (cont'd.)

Gage		Total Load in Lbs.									
		Side A (outside)					Side B (inside)				
		0	100	200	300	400	0	100	200	300	400
11	R	1552	1549	1545	1541	1538	1092	1138	1184	1230	1277
	W	1340	1302	1262	1222	1182	1162	1172	1182	1192	1202
	B	914	848	778	707	632	922	872	817	762	708
12	R	1297	1281	1265	1247	1229	1070	1132	1201	1268	1336
	W	1250	1193	1132	1071	1008	1510	1539	1570	1600	1632
	B	1378	1305	1225	1143	1065	1470	1421	1372	1322	1270
13	R	1231	1210	1187	1163	1140	1248	1342	1445	1547	1650
	W	1579	1488	1387	1292	1192	1402	1453	1511	1564	1622
	B	1502	1412	1317	1222	1121	940	900	860	820	778
14	R	1000	1049	1102	1155	1210	1000	1130	1269	1409	1548
	W	1000	1018	1038	1058	1079	1000	1034	1071	1108	1147
	B	1000	885	761	640	516	1000	925	842	759	673
15	R	1558	1563	1571	1577	1582	1433	1361	1281	1204	1124
	W	1322	1415	1513	1610	1709	1208	1173	1139	1108	1074
	B	1355	1449	1548	1648	1752	1092	1122	1155	1188	1222
16	R	1250	1263	1278	1293	1309	1059	1009	953	901	847
	W	1432	1486	1548	1603	1665	1269	1250	1231	1212	1192
	B	1428	1488	1553	1618	1682	000	040	086	128	170
17	R	1765	1772	1782	1792	1802	1362	1321	1277	1232	1187
	W	1397	1433	1472	1512	1552	1378	1368	1358	1348	1338
	B	1659	1717	1778	1839	1900	1178	1221	1267	1311	1360
18	R	1610	1621	1633	1645	1657	1634	1592	1549	1503	1458
	W	1270	1299	1329	1357	1388	1559	1553	1550	1545	1540
	B	1589	1648	1709	1770	1831	1449	1488	1530	1571	1612
19	R	1117	1131	1145	1158	1170	1532	1478	1416	1358	1299
	W	1775	1797	1819	1839	1860	1295	1287	1278	1269	1260
	B	332	399	466	531	600	1729	1764	1802	1840	1878

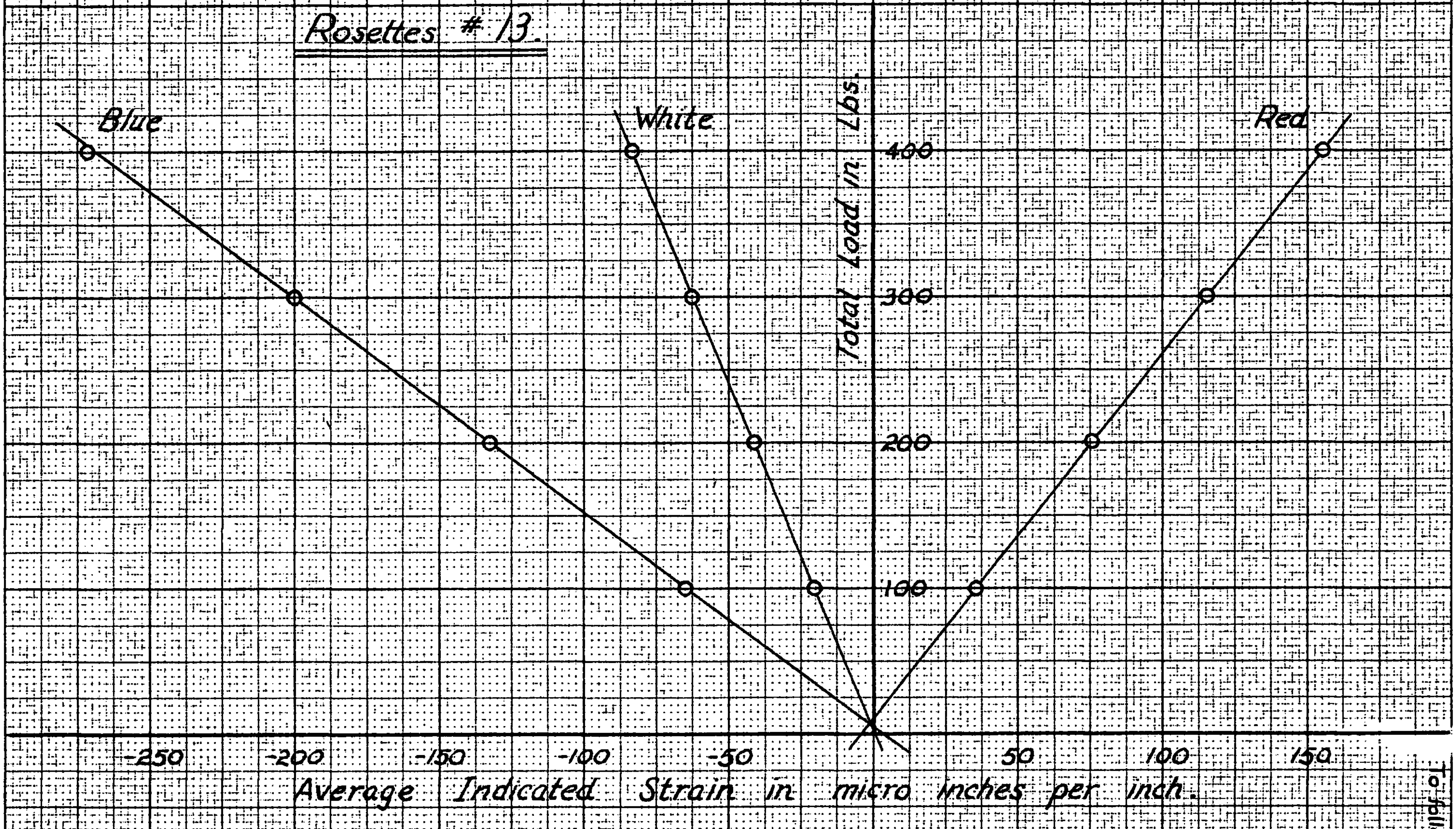

Fig. 4-2.

To follow 65

PRINTED IN U S A

EUGENE DIETZGEN CO. NO. 346 BX

The slope of the line was determined from the graph and then corrected for the Gage Factor by Equation 4 - 1. Mohr's circles of strain were then plotted for a total load on the shell of 100 pounds. Strains were converted to stresses by superimposing Mohr's circle of stress over that for strain. The results for a typical rosette are shown in Figure 4 - 3. Since the superposition of Mohr's circle of stress over the circle of strain is not too common, a brief discussion is included here.

Normal strains, denoted by ϵ, are positive when they are elongations. Shearing strains, denoted by γ, are positive when the originally rectangular element is distorted with respect to the co-ordinate axes as shown in Figure 4 - 4. Then the strain on

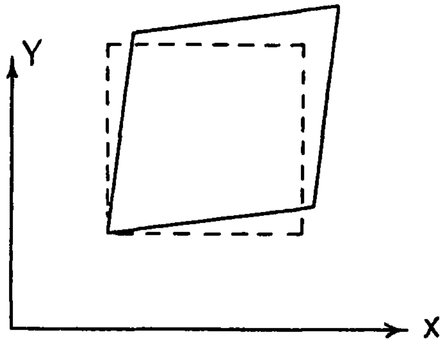

Fig 4 - 4

a plane whose outward normal is at a counter clockwise angle θ to the X axis is

$$\left.\begin{aligned} \epsilon_\theta &= \frac{\epsilon x + \epsilon y}{2} + \frac{\epsilon x - \epsilon y}{2} + \frac{\gamma xy}{2} \sin 2\theta \\ \gamma_\theta &= (\epsilon y - \epsilon x) \sin 2\theta + \gamma xy \cos 2\theta \end{aligned}\right\} \quad (4 - 2)$$

Referring to the principal axes of strain rather than the X and Y axes, Equations (4-2) become

$$\left.\begin{aligned} \epsilon_\alpha &= \frac{\epsilon \max + \epsilon \min}{2} + \frac{\epsilon \max - \epsilon \min}{2} \cos 2\alpha \\ \gamma_\alpha &= (\epsilon \min - \epsilon \max) \sin 2\alpha \end{aligned}\right\} \quad (4 - 3)$$

where α is the counterclockwise angle from the positive principal strain axis to the outward normal of the plane under consideration.

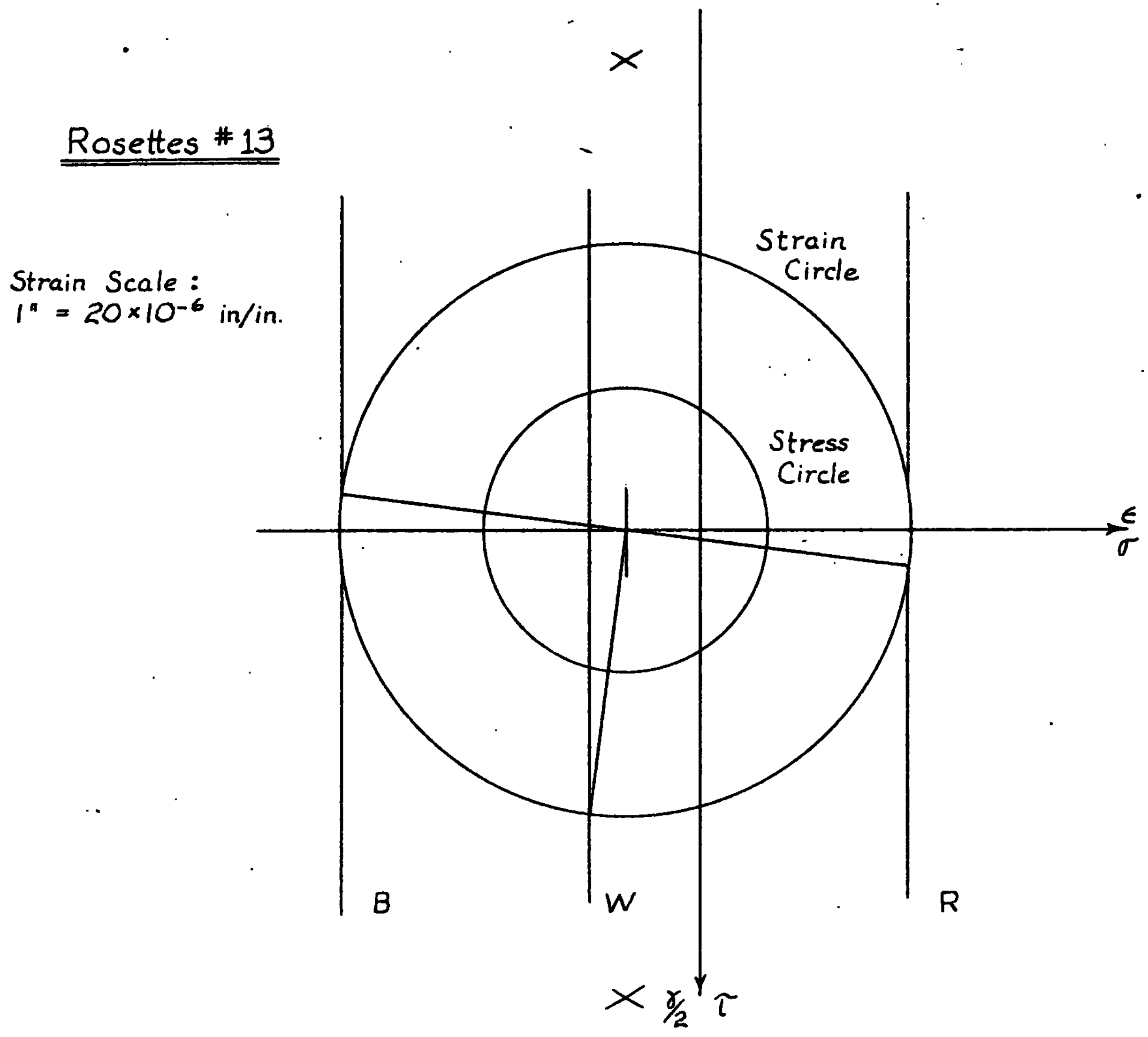

Fig. 4 - 3.

To follow 66.

Let

$$\frac{\epsilon_{max} + \epsilon_{min}}{2} = A$$

and

$$\frac{\epsilon_{max} - \epsilon_{min}}{2} = B \qquad (4 - 4)$$

then Equations (4 - 3) reduce to

$$\begin{aligned} \epsilon_\alpha &= A + B \cos 2\alpha \\ \gamma_\alpha &= - 2 B \sin 2\alpha \end{aligned} \qquad (4 - 5)$$

Mohr's circle of strain is a plot of ϵ as abscissa, positive to the right, and $\frac{\gamma}{2}$ as ordinate, positive down. From equations (4 - 5), it can be seen that A is the distance from the origin to the centre of Mohr's circle of strain and B is the radius of the circle.

Considering stresses as positive when producing positive strain, the stress equations are very similar to the strain equations. Referring the stress or any plane to the principal stress axes, the stress equations are

$$\begin{aligned} \sigma_\alpha &= \frac{\sigma_{max} + \sigma_{min}}{2} + \frac{\sigma_{max} - \sigma_{min}}{2} \cos 2\alpha \\ \tau_\alpha &= \frac{\sigma_{min} - \sigma_{max}}{2} \sin 2\alpha \end{aligned} \qquad (4 - 6)$$

But

$$\begin{aligned} \sigma_{max} &= \frac{E}{1-\mu^2} \left[\epsilon_{max} + \mu \epsilon_{min} \right] \\ \sigma_{min} &= \frac{E}{1-\mu^2} \left[\epsilon_{min} + \mu \epsilon_{max} \right] \end{aligned} \qquad (4 - 7)$$

Substituting Equations (4 - 7) and (4 - 4) into Equations (4 - 6), the stress equations become

$$\left.\begin{aligned} \sigma_\alpha &= \frac{E}{1-\mu}\left[A + \left(\frac{1-\mu}{1+\mu}\right) B \cos 2\alpha\right] \\ \tau_\alpha &= \frac{E}{1-\mu}\left[-\left(\frac{1-\mu}{1+\mu}\right) B \sin 2\alpha\right] \end{aligned}\right\} \quad (4-8)$$

Comparing Equations (4 - 8) with Equations (4 - 5) show that if the stress scale is $\frac{E}{1-\mu}$ times the strain scale, Mohr's circles of stress and strain are concentric. Furthermore the radius of the stress circle is $\frac{1-\mu}{1+\mu}$ times the radius of the strain circle.

A piece of Perspex approximately 1/8" thick, 2½" wide and 17" long was cut from the same material as was used for the model. Two strain rosettes were attached, one on each side. The specimen was submitted to a tensile test in the Baldwin-Southwark Testing Machine. From the readings recorded, graphs were plotted and the elastic properties calculated. The results of the tests are

$$E = 4.64 \times 10^5 \ \text{lb/in}^2$$

$$\mu = .337 \sim \frac{1}{3}$$

Referring to Equations (4 - 8) and using the determined elastic properties show that the radius of Mohrs circle of stress is $\frac{1-\frac{1}{3}}{1+\frac{1}{3}} = \frac{1}{2}$

the radius of Mohr's circle of strain. The co-ordinates of any point on the stress circle are measured using the strain circle scale and then multiplied by $\frac{4.64 \times 10^5}{1 - \frac{1}{3}} = .695 \times 10^6$.

While part of the quantitative experimental results are disappointing, the overall results are reasonable. The application of smooth shell theory to this type of folded plate shell does seem justified. Any slight discrepancy between theory and experiment in the model is greater than the corresponding discrepancy in a shell composed of more triangles because the latter is a closer approximation of a smooth shell. Therefore, to obtain the maximum membrane stress in a folded plate shell, the smooth shell membrane stress is multiplied by the appropriate stress riser from Graph 4 - 1.

D. RESULTS

From Mohr's circle, the normal and shear stresses were determined on the planes parallel to the edges of the triangle. The resulting stress distribution curves are shown in Figures (4 - 5 and (4 - 6). These curves prove that the stress distribution is not linear as in smooth shells but rather a parabolic shape. There is an unsymmetrical normal stress reversal near the upper vertex on the side of the triangle lying in the meridian. This peculiarity may perhaps be explained by the fact that part of the load was applied at the vertex of the triangle. The proximity of the concentrated load may result in secondary effects at this point. Except for this one point the rest of the points appear to plot as relatively smooth curves.

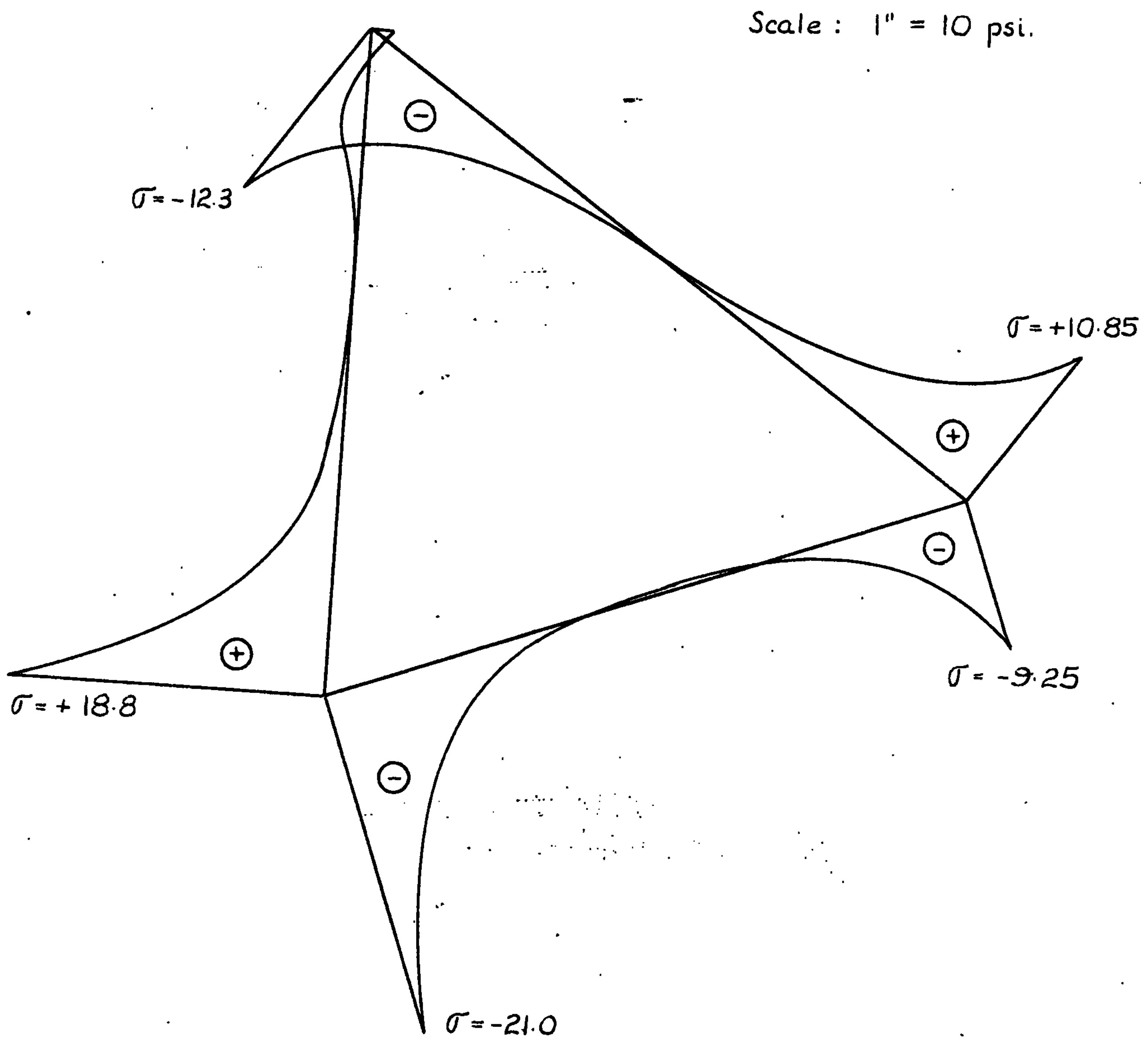

Fig 4 - 5 Distribution of Normal Stress in p.s.i. on the Gage Line Triangle

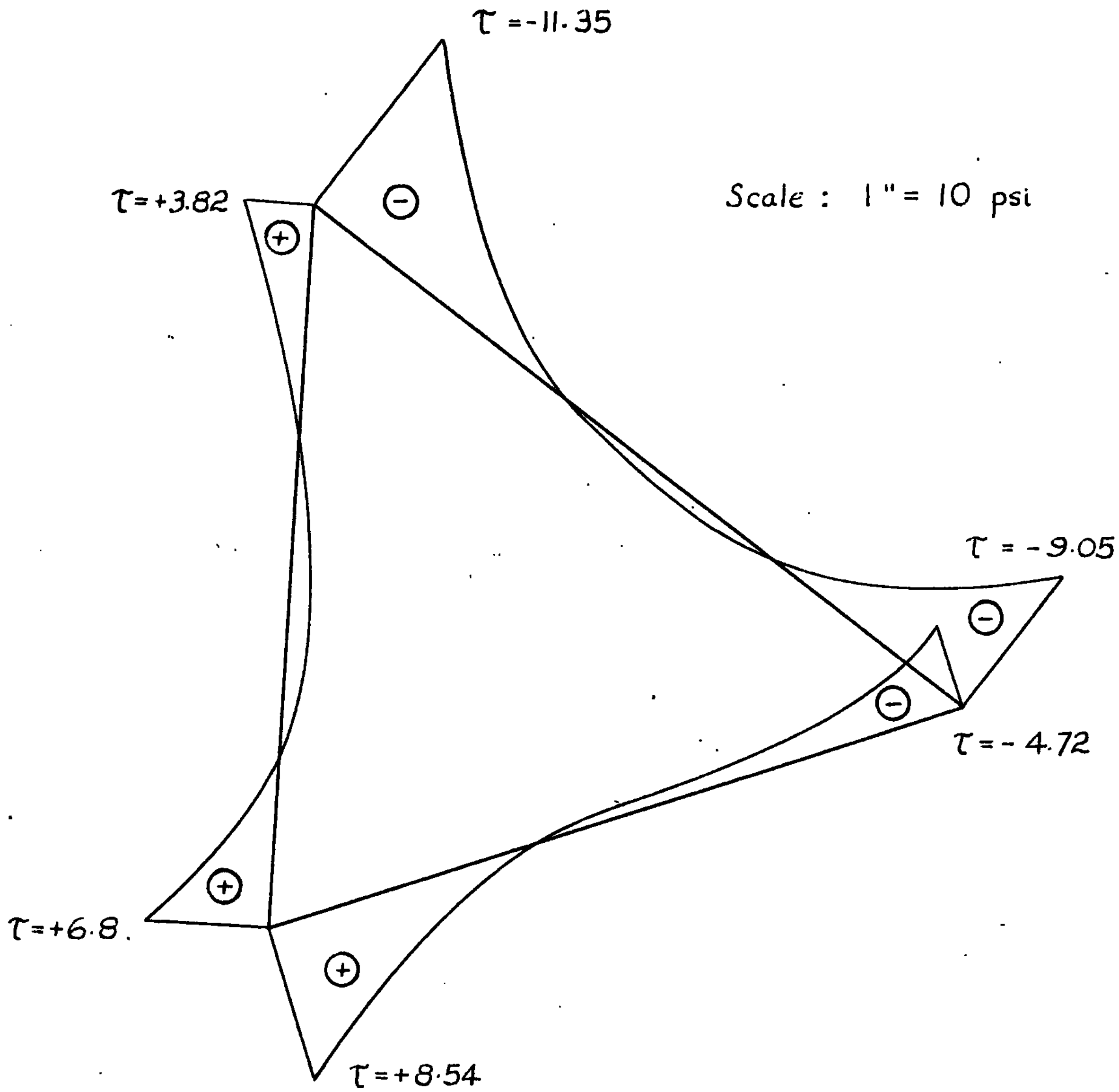

Fig 4 - 6 Distribution of Shear Stress in the RB plane of the Gage Line Triangle

In order to check the accuracy of the experimental work, the curves of Figures (4 - 5) and (4 - 6) were plotted to a much larger scale on graph paper. The area under the curves was determined and then replaced by concentrated forces and moments as shown in Figure (4 - 7). The forces shown are all in the same plane so there are three equations of equilibrium. Taking an arbitrary set of axes as shown and writing the three equations gives

$$\Sigma X = +4.21 - 5.16 = -0.95 \text{ lb}$$

$$\Sigma Y = +4.04 - 3.86 = +0.18 \text{ lb}$$

$$\Sigma M = +71.49 - 64.95 = +6.54 \text{ in.lb}$$

The additional force required for equilibrium acts as shown in the Figure. The results of the sum of the forces in the X direction is not particularly good. However the results of the ΣY and the ΣM are fairly good with an error of 4½% and 9½% respectively.

To compare the experimental forces to the theoretical forces, the gage lines must be produced to the actual boundary of the triangle. This results from the fact that the membrane force distribution in the folded plate shell is not linear, the majority of the force being near the edge of the triangle. In computing the theoretical forces, Equation (1 - 2) was used. It was refined slightly by using for ϕ, the actual slope of the particular plane triangle and not the ϕ for the spherical triangle. This procedure is justified in this case because the model is a much poorer approximation of a sphere than one formed of more triangles. The results are shown in Fig 4 - 8. Though there is a slight displacement of the normal forces, numerically, they agree very well.

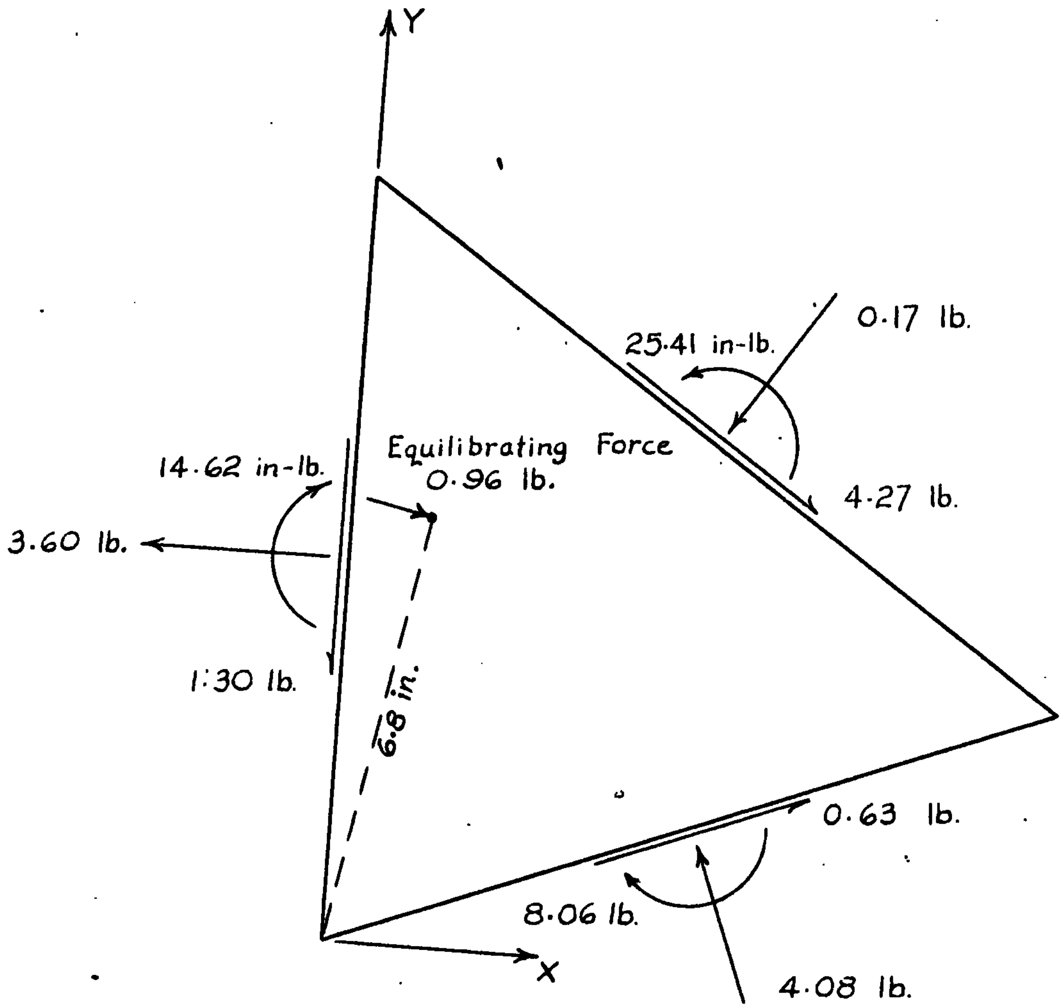

Fig 4 - 7 Resultant Forces on Gage Line Triangle

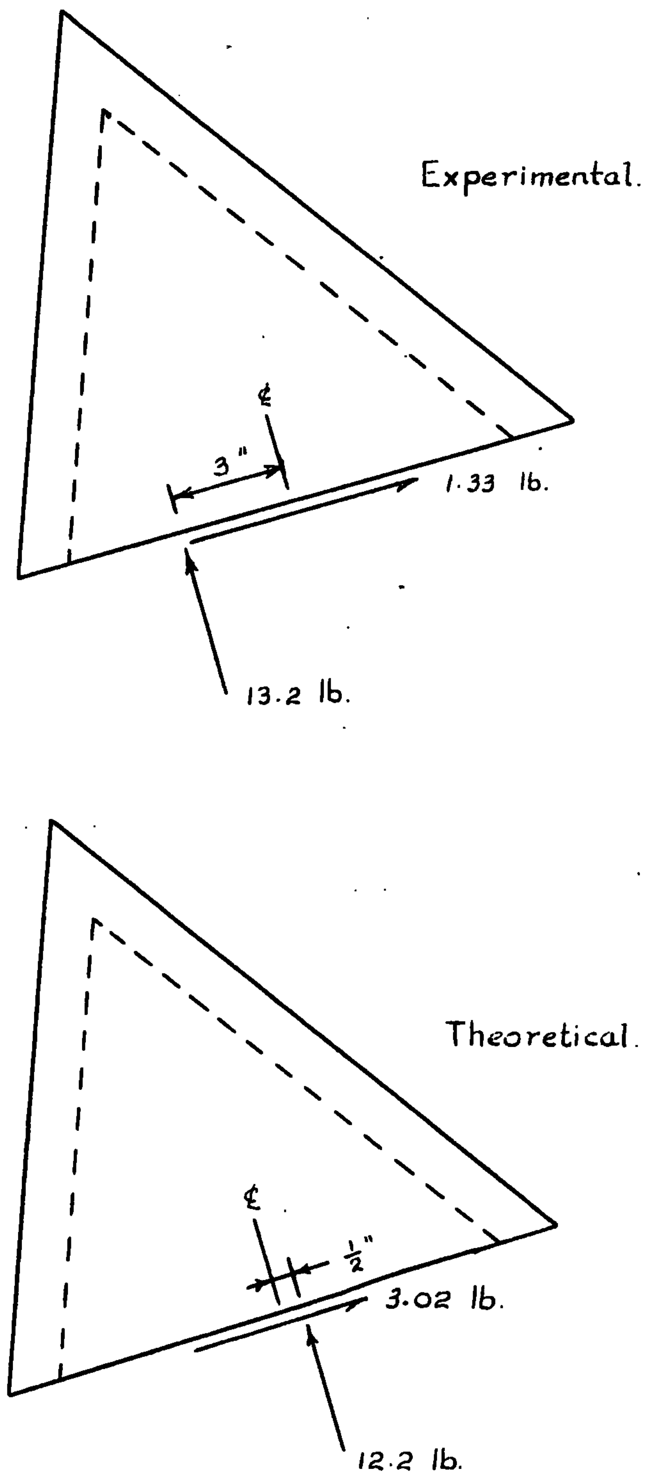

Fig 4 - 8 Comparison of Experimental and Theoretical Results.

That the loads on the shell are supported by membrane action and not bending action may be demonstrated in yet another way. A transit set up thirteen feet from the model was sighted on the crown where part of the load was applied as a concentrated force. When the full load of 400 pounds was applied to the shell, this point deflected only two hundredths of an inch. This deflection was verified more accurately using a dial gage. Similarly, the transit was sighted on a point of the model where $\varphi \approx 60^{\circ}$. Under full load, no vertical or radial deflection was observed since any deflection that did occur was so slight that it was obscured by the transit cross hairs. These deflections show that the loads are carried predominantly by membrane action because bending would produce larger deflections. There may be some bending action however, beneath the concentrated loads.

The stress riser was determined from large scale curves of Figure 4 - 5. These curves were produced to the boundary of the actual triangle. The area under approximately one half the curve was determined and converted to an average stress. Then the stress riser is

$$K_{SR} = \frac{\sigma_{max.}}{\sigma_{ave.}}$$

The results are plotted in Graph 4 - 1. There are only five points plotted instead of six because of the unsymmetrical stress reversal discussed previously. When the deflection angle is 180°, the stress riser is equal to one as in a smooth shell. This enables a fairly good curve to be drawn despite the fact most of the experimental points plotted are for relatively small dihedral angles.

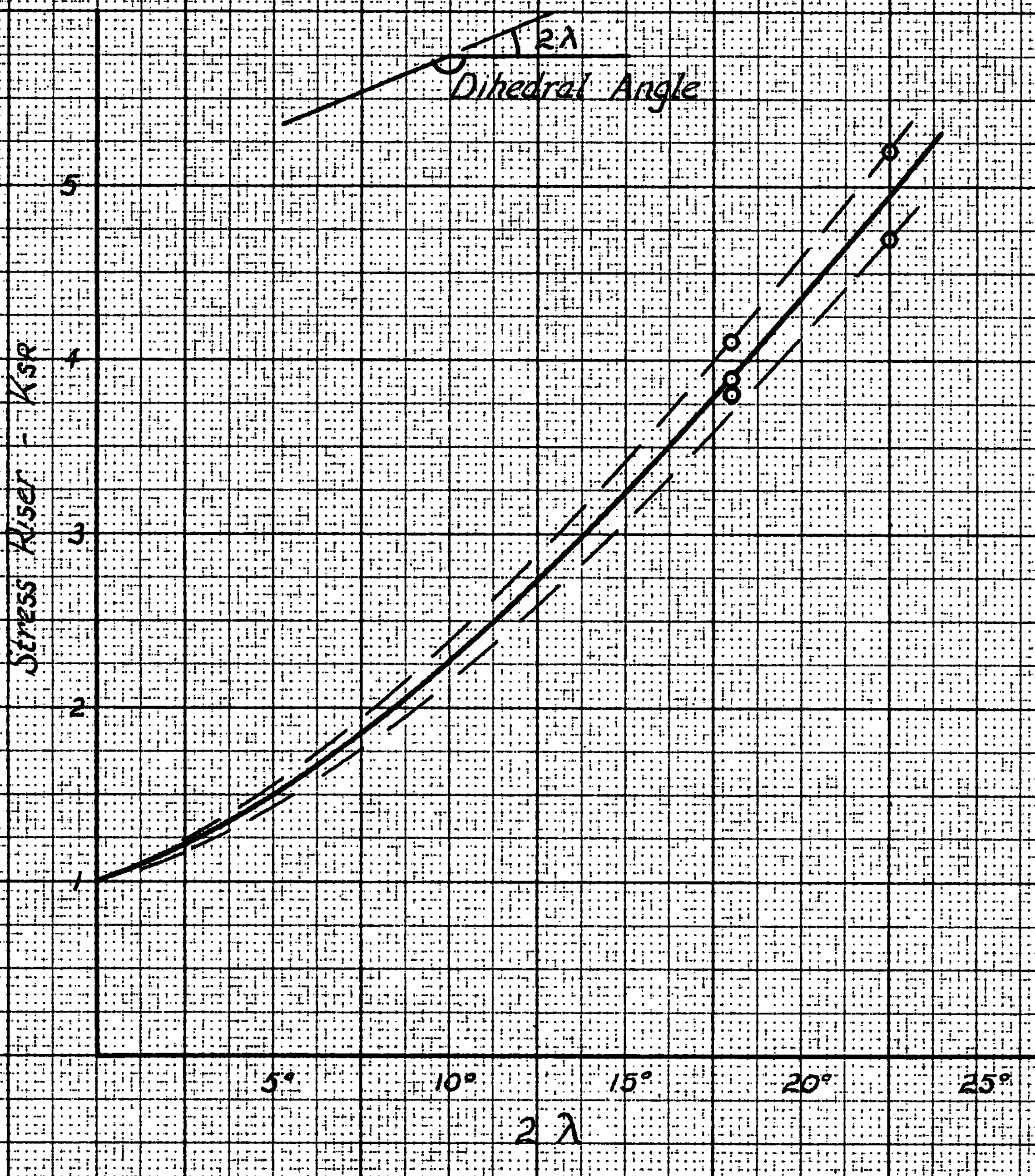

Graph 4-1

CHAPTER V

DESIGN OF A PLYWOOD GEODESIC SHELL

A. INTRODUCTION

After ths size and shape of the spherical shell have been determined, the geodesic geometry may be selected with the aid of Figure 2 - 8. As this Figure gives only average values, the triangles should be laid out accurately and the altitudes scaled as a check that the triangles can be cut from a four foot wide panel. Less material is wasted if the triangles are cut from panels longer than the standard eight feet. Since long panels are more expensive per square foot, the economy between the two alternatives should be investigated.

When the dead load has been estimated and the live loads determined, the membrane forces from each load are computed individually using smooth shell theory. Graphs 1 - 1 and 1 - 2 may be of use for this determination. The membrane forces from the various loads are then combined to give the largest numerical membrane force for a given angle φ. Since the largest membrane stress occurs at the vertices of the triangle, the smooth shell stress at this point must be multiplied by the appropriate stress riser from Graph 4 - 1.

At interior points in the triangle, the membrane stresses are combined with the stresses arising from lateral loads on the triangle. Since these points are remote from the vertices, the membrane stresses are not multiplied by a stress riser.

The forces required for buckling of the triangle and the dome must also be computed and compared to the actual membrane forces. Buckling is caused by an average force on the triangle so that no stress riser is used. Buckling probably will occur within the elastic range and may govern the design. The factor of safety against buckling should not be less than four.

DESIGN NOTES

for

PLYWOOD FOLDED PLATE HEMISPHERE

WITH A 28' RADIUS.

Geometry:

The hemisphere may be formed from 640 triangles of ten kinds using the geometry from Table 2 - 4. An accurate check of the geometry shows that the equilateral triangle has the largest altitude. For a 28 foot radius, this altitude is four feet and the triangles may be cut from the standard four foot width panel.

Dead Load:

Plywood	2 psf
Battens, waterproofing interior facing and lighting	3
	5 psf

Live Load:

The National Building Code for the Vancouver area gives:

(a) Snow Load - 40 psf of horizontal area

(b) Wind - 90 mph gust velocity

At a height of 20 feet above the ground, the Code gives a wind force of 18.5 $\approx$ 20 psf. of which approximately half is distributed on each side of the structure. Therefore for External wind use $p = 10$ psf. Wind action may also produce a uniform internal radial force, either in or out, of $.2(20) = 4$ psf.

Membrane Forces in lbs/ft (Forces marked * do not occur simultaneously.)

φ	Dead Load		Snow Load		Ext. Wind.		Int. Wind		Abs. Max. (no wind)		Abs. Max. (wind) $\theta = 0°$		Wind $\theta = 90°$
	N_φ	N_θ	N_φ	N_θ	N_φ	N_θ	N_φ	N_θ	N_φ	N_θ	N_φ	N_θ	$N_{\varphi\theta}$
0°	-70	-70	-600	-600	0	0	±56	±56	-670	-670	-726	-726	0
10°	-71	-67	-600	-564	±12	±37	"	"	-671	-631	-739	-724	±12
20°	-73	-59	-600	-460	±24	±72	"	"	-673	-519	-753	-647	±25
30°	-75	-46	-576	-198	±33	±107	"	"	-651	-244	-740	-407	±38
40°	-79	-28	-528	+60	±41	±139	"	"	-607	+60	-704	+255	±53
50°	-86	-4	-468	+264	±45	±170	"	"	-554	*+264	-655	*+490	±70
60°	-94	+23	-408	+360	±44	±198	"	"	-502	+383	-602	*+637	±90
70°	-104	+56	-354	+354	±39	±224	"	"	-458	+410	-553	*+690	±114
80°	-119	+95	-318	+318	±25	±251	"	"	-437	+413	-518	*+720	±145
90°	-140	+140	-295	+295	0	±280	"	"	-435	+435	-491	*+771	±187

Assume 5/8" Sanded, Douglas Fir Plywood, Good 1 Side

This size plywood has five veneers; two faces each 1/10" thick, two cores perpendicular to the face each 1/6" thick, and one centre core parallel to the face 1/6" thick. The properties for a 12 inch width, where n and t are the axes parallel and perpendicular to the face grain respectively, are:

$A_n = 3.47 \text{ in}^2$	$A_t = 4.03 \text{ in}^2$
$Z_n = 0.388 \text{ in}^3$	$Z_t = 0.488 \text{ in}^3$
$I_n = 0.121 \text{ in}^4$	$I_t = 0.123 \text{ in}^4$

The allowable working stresses in psi for dry location are:

Tension	$\sigma_n = \sigma_t = 1875$
Compression	$\sigma_n = \sigma_t = 1360$
Shear through the thickness	$\tau_{nt} = \tau_{tn} = 192$
Rolling Shear	$\tau_{zn} = \tau_{zt} = 72$

No Wind

The maximum stresses in a triangle from a lateral snow load occurs when $\varphi \leq 20^{\circ}$. One severe combination of membrane forces act at $\varphi = 0^{\circ}$. Therefore, the triangle adjacent to the crown must be analysed. The average membrane forces are $N\varphi = N\theta = -670$ lbs/ft and $N\varphi\theta = 0$ and the lateral snow load is 40 lb/ft^2. The points to be analysed are shown in the Figure.

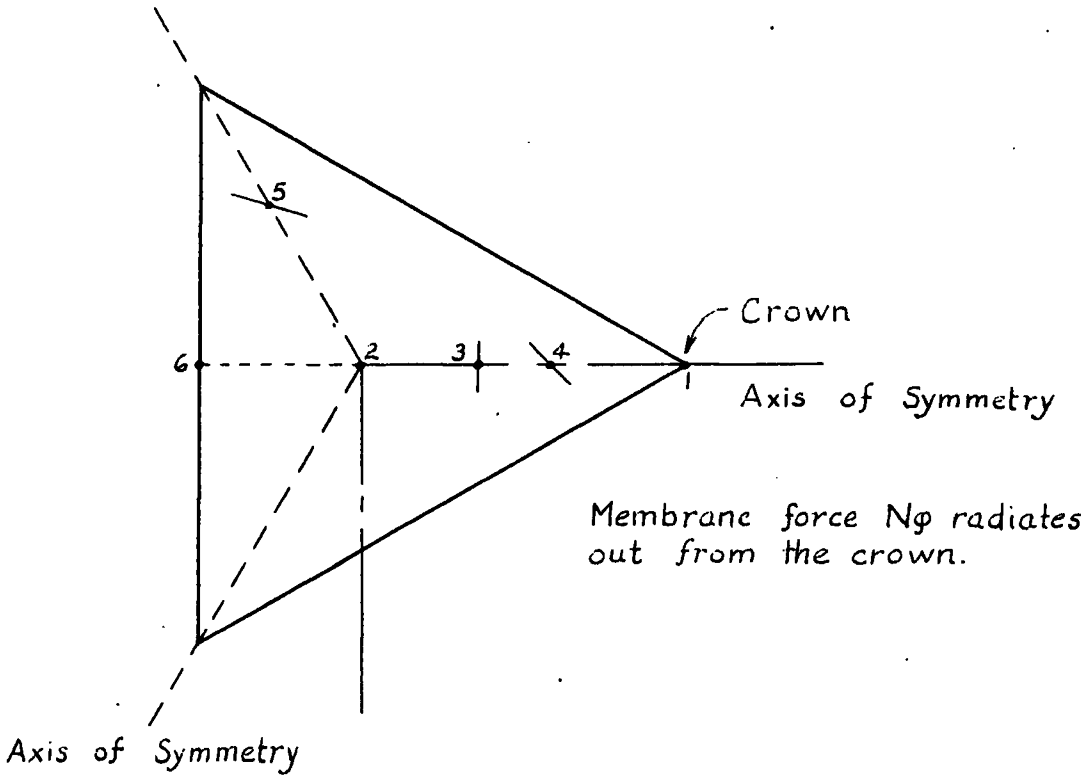

Point 1

The combination of membrane stresses is a maximum at this point. Mohr's circle is a point. From Figure 4 - 9, $K_{SR} = 1.7$. Therefore the stresses are

$$\sigma_n = -\frac{670\ (1.7)}{3.47} = -328 \text{ psi}$$

$$\sigma_t = -\frac{670\ (1.7)}{4.03} = -283 \text{ psi}$$

$$\tau_{nt} = 0$$

Substituting into Equation 3 - 30 gives

$$\left(\frac{328}{1360}\right)^2 + \left(\frac{283}{1360}\right)^2 + \left(\frac{0}{192}\right)^2 = .058 + .043 = .101 \ll 1$$

Point 2

At the centroid of the triangle $M_x = M_y = 14.8$ lbs. Mohr's circle of moments is a point and Mohr's circle of membrane stress is also a point so that the same stresses occur on all planes considered. From Equations 3 - 31 the stresses are

$$\sigma_n = -\frac{670}{3.47} + \frac{14.8\ (12)}{.388} = -193 \pm 457 = -650 \text{ psi}$$

$$\sigma_t = -\frac{670}{4.03} + \frac{14.8\ (12)}{.488} = -166 + 364 = -530 \text{ psi}$$

$$\tau_{nt} = 0$$

$$\left(\frac{650}{1360}\right)^2 + \left(\frac{530}{1360}\right)^2 = .228 + .152 = .380 < 1$$

Point 3

At this point My is a maximum but Mx = 0 The severe orientation of the plywood is when the n axis is coincident with the y axis. Then Mn = 16 lb and Nn = Nt = - 670 $^{lb}/ft$. The stresses are

$$\sigma n = -\frac{670}{3.47} \pm \frac{16\ (12)}{.388} = -193 \pm 495 = -688 \text{ psi}$$

$$\sigma t = -\frac{670}{4.03} \pm 0 = -166 \text{ psi}$$

$$\tau nt = 0$$

Then

$$\left(\frac{688}{1360}\right)^2 + \left(\frac{166}{1360}\right)^2 = .257 + .015 = .272 < 1$$

Point 4

At this point Mnt is a maximum when the n axis is 45^o to the x axis. Mohr's circle of membrane stress is a point so Nn and Nt act also. The values of the moments and forces are

$$Mnt\Big]_{\alpha = 45^o} = \pm .234 \frac{a^2}{16} (1 - u) = 9.35 \text{ lbs}$$

$$Mn\Big]_{\alpha = 45^o} = .05 \frac{q a^2}{8} = 4 \text{ lbs}$$

$$Nn = Nt = -670 \ ^{lb}/_{ft.}$$

The stresses are

$$\sigma n = -\frac{670}{3.47} \pm \frac{4(12)}{.388} = -193 - 124 = -317 \text{ psi}$$

$$\sigma t = -\frac{670}{40} \pm \frac{4(12)}{488} = -166 - 98 = -254 \text{ psi}$$

$$\tau nt = \pm 9.35 \ \frac{6}{h^2} = \frac{9.35\ (6)\ 64}{25} = 144 \text{ psi}$$

Then

$$\left(\frac{317}{1360}\right)^2 + \left(\frac{254}{1360}\right)^2 + \left(\frac{144}{192}\right)^2 = .054 + .038 + .563 = .655 < 1$$

Point 5

By symmetry, Mnt is also a maximum here. However, since Mohr's circle of normal stress is a point, the combined stress is the same as at Point 4.

Point 6

At this point Q is a maximum giving the largest rolling shear. The value of Q_{max} is $\frac{q\,a}{4}$. Before determining the rolling shear stress, the first moment of area at the innermost glue line must be computed.

Point 6 (Cont'd)

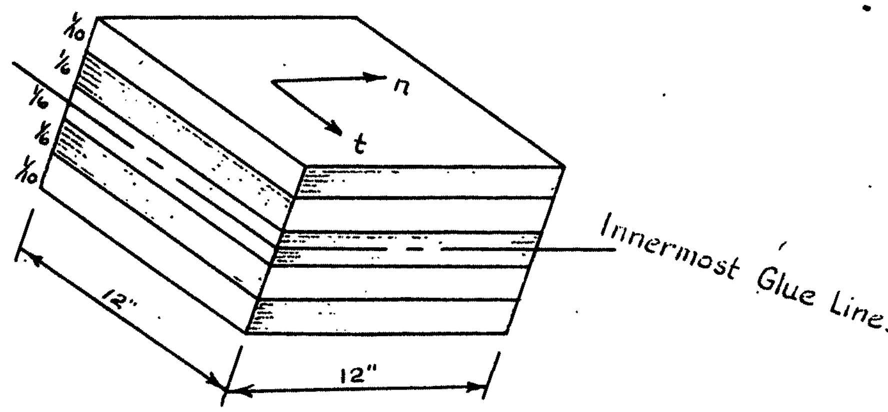

$$S_n = \frac{1}{10}(12) \times \left(\frac{1}{20} + \frac{1}{6} + \frac{1}{12}\right)$$

$$= \frac{12}{10} \times \frac{18}{60} = \frac{9}{25}\ \frac{in^3}{ft}$$

$$S_t = \frac{1}{6}(12) \times \frac{1}{6} = \frac{1}{3}\ \frac{in^3}{ft}$$

Therefore the stresses are

$$\tau_{zn} = \frac{Q_n S_n}{I_n W} = \frac{a}{4}\ \frac{S_n}{I_n W} = \frac{40(4)}{4}\ \frac{9}{25}\ \frac{1}{(121)12} = 9.9 \text{ psi} < 72$$

$$\tau_{zt} = \frac{Q_t S_t}{I_n W} = 40\ \frac{1}{3}\ \frac{1}{.123(12)} = 9.0 \text{ psi} < 72$$

Reviewing the points just analysed, it is noted that the shear stress from twisting moments is largely responsible for producing the most severe combination of stress. Therefore if the twisting moment remains constant and additional membrane shear stresses occur, a more severe stress condition may result. Such a condition may occur at Point 4 when the triangle is at $\varphi = 20^{\circ}$. In this position the lateral load is still 40 psf but Mohr's circle is no longer a point and is as shown in the Figure. On the plane with maximum shear, the

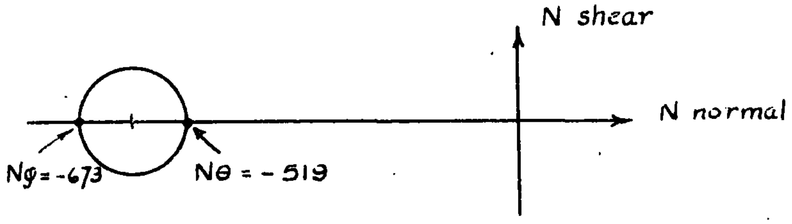

shear force is $\frac{N\varphi - N\theta}{2} = -77\ ^{lb}/_{ft.}$ and the normal force is $\frac{N\varphi + N\theta}{2} = -596\ ^{lb}/_{ft.}$

Point 4 $\varphi = 20^{\circ}$

The most severe stresses occur when maximum membrane shear and maximum twisting moment occur on the same plane. The moments are the same as before so the forces and moments are:

$$Nn = Nt = -596\ ^{lb}/_{ft}$$

$$Nnt = 77\ ^{lb}/_{ft.}$$

$$Mn = 4\ lb$$

$$Mnt = 93.5\ lb$$

Therefore the stresses are

$$\sigma_n = -\frac{596}{3.47} \pm \frac{4(12)}{.388} = -172 - 124 = -296 \text{ psi}$$

$$\sigma_t = -\frac{596}{4.03} \pm \frac{4(12)}{.488} = -148 - 98 = -246 \text{ psi}$$

$$\tau_{nt} = \frac{77}{7.5} + 93.5\,(6)\left(\frac{8}{5}\right)^2 = 10 + 144 = 154 \text{ psi}$$

Then

$$\left(\frac{296}{1360}\right)^2 + \left(\frac{246}{1360}\right)^2 + \left(\frac{154}{192}\right)^2 = .048 + .033 + .642$$

$$= .723 < 1$$

For φ greater than 20°, the membrane shear force becomes larger but the twisting moment becomes smaller. The net effect produces a less severe stress condition. While the worst stress combination may not have been evaluated, its value will vary only a little from point 4. Since the allowable increase is comparatively large before the left hand side of Equation 3 - 30 is greater than unity, it is not necessary to carry the investigation further for the case when no wind is acting.

WIND ACTING

In practise, an increase in the allowable stress may be permitted for wind action. Even if no increase in stress is permitted, it does not appear necessary to investigate Points 1, 2, 3 and 6 since the factor of safety is so large. To illustrate the analysis for wind, only one point will be investigated.

Point 4 $\varphi = 20^\circ \quad \theta = 0^\circ$

The lateral loads on the triangle are caused not only by snow loads but also by internal and external wind pressure. The lateral loads are

Dead Load	=			5
Snow	=			40
Int. Wind	=	.2 (20)	=	4
External	=	p sin φ	= 10 sin 20° =	3.5
			q	= 52.5 psf

The membrane forces are

$$N\varphi = -753 \ {}^{lb}/_{ft}$$

$$N\theta = -647 \ {}^{lb}/_{ft}$$

Taking as before the most severe stress condition when maximum membrane shear and maximum twisting moment occur on the same plane, the forces and moments are :

$$Nn = Nt = -\frac{753-647}{2} = -\frac{1400}{2} = -700 \ {}^{lb}/_{ft.}$$

$$Nnt = -\frac{753+647}{2} = -\frac{106}{2} = 53 \ {}^{lb}/_{ft.}$$

$$Mnt = \pm .234 \frac{q a^2}{16}(1-u) = .234 (52.5) \frac{16}{16} = 12.3 \text{ lbs.}$$

$$Mn = .05 \frac{q a^2}{8} = .05 (52.5) \frac{16}{8} = 5.25 \text{ lbs.}$$

The stresses are:

$$\sigma n = - \frac{700}{3.47} \pm \frac{5.25(12)}{.388} = -202 \pm 157 = -359$$

$$\sigma t = - \frac{700}{4.03} \pm \frac{5.25(12)}{.488} = -174 \pm 129 = -303$$

$$\tau nt = - \frac{53}{7.5} \pm 12.3(6)\left(\frac{8}{5}\right)^2 = -7 \pm 188 = -195$$

Then

$$\left(\frac{359}{1360}\right)^2 + \left(\frac{303}{1360}\right)^2 + \left(\frac{195}{192}\right)^2 = .070 + .050 + 1.01$$

$$= 1.13 > 1$$

A 13% increase in stress is not unreasonable for such short term loading.

<u>Buckling of Triangle</u> (Equilateral triangle is critical)

$$D = EI = 1.8\,(10^6)\left(\frac{.121}{12}\right) = 1.815\,(10^4) \quad \text{lb - in}$$

From Fig 3 - 11, $K = 4.75$

$$b = 48\,\frac{(2)}{\sqrt{3}} = 55.4 \text{ in}$$

$$(Nx)cr = K\,\frac{\Pi\,D}{b^2}$$

$$= -\,4.75\,\frac{\Pi^2\,(1.815)(10^4)}{(55.4)^2} = 277\,\frac{\text{lb}}{\text{in}}$$

$$= 3320\,\frac{\text{lb}}{\text{ft}}$$

Factor of safety is $\frac{3320}{726} = 4.5$

which is satisfactory.

<u>Buckling of Dome</u>

$$\frac{\sigma \rho}{Eh} = .183$$

$$\therefore\ Ncr = .183\,\frac{E\,heff^2}{\rho}$$

$$= .183\,\frac{(1.8)(10^6)(.496)^2}{28} = 2890\,\frac{\text{lb}}{\text{ft}}$$

Factor of safety is $\frac{2890}{726} = 4.0$

which is satisfactory.

Design of Marginal Beams

If the beams are nail glued to the triangles, the membrane force is transmitted to the beam by rolling shear. This governs the width of the beam. The membrane force is transmitted to the next triangle in the beam by tension or compression perpendicular to its length. This governs the depth. Since wood is weak in tension perpendicular to the grain, plywood should be used since some laminae will have their grain parallel to the stress. Some bending of the beam may also occur but this is small and may be neglected.

Max membrane force is + 771 lb/ft.

Ks = 1.7

Max force is 1.7(771) = 1310 lb/ft.

Allowable stress in rolling shear is 72 psi

Total width of beam is

$$2 \frac{1310}{72(12)} = 3.04 \text{ in}$$

Use minimum width of 4 inches to facilitate nailing.

Assume 5/8 S Plywood with face grain parallel to the joint.

Area perpendicular to face grain is 4.03 in^2

Therefore tension stress is

$$\frac{1310}{4.03} = 325 < 1875 \text{ O.K.}$$

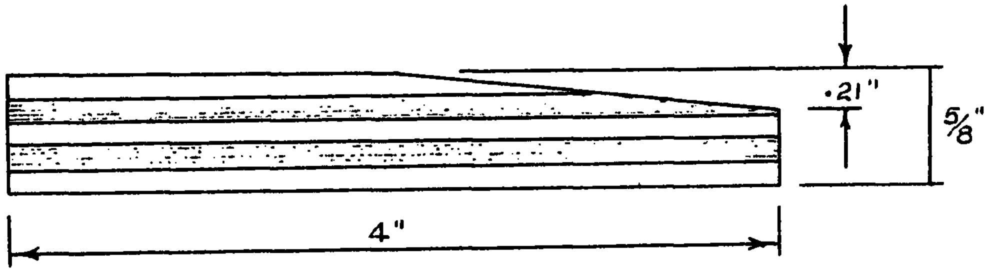

Fig 5 - 2 Cross Section of Typical Beam.

BIBLIOGRAPHY

A. Books

Allen, D. N. deG. Relaxation Methods. New York, McGraw-Hill, 1954.

Army-Navy-Civil Committee. A. N. C. Handbook on the Design of Wood Aircraft Structures. Washington, U.S.Department of Agriculture, 1942.

Cundy, H. M. and Rollett, A.P. Mathematical Models. Oxford, Clarendon Press,1952.

Flugge, W. Statik und Dynamik der Schalen, Berlin, 1934

Forest Products Laboratory. Wood Handbook. Washington, U.S.Department of Agriculture, 1955.

Hetenyi, M. I. ed. Handbook of Experimental Stress Analysis. New York, Wiley,1950

Lee, G. H. An Introduction to Experimental Stress Analysis, New York, Wiley, 1950

Perry, C. C. and Lissner, H. R., Strain Gage Primer, New York, McGraw-Hill,1955

Timoshenko, S. Theory of Plates and Shells. New York, McGraw-Hill, 1940

Timoshenko, S. and Goodier, J. N. Theory of Elasticity. New York, McGraw-Hill,1951

Timoshenko, S. Theory of Elastic Stability. New York, McGraw-Hill, 1936

Timoshenko, S. and MacCullough, G. H. Elements of Strength of Materials. New York, Van Nostrand, 1949.

B. Periodicals

Bossart, K. J. and Brewer, G. A. "A Graphical Method of Rosette Analysis". Proceedings of the Society for Experimental Stress Analysis. Vol. 4, No. 1. (1946), pp.1 - 8

Hewson, T. A. "A Nomographic Solution to the Strain Rosette Equations". Proceedings of the Society for Experimental Stress Analysis. Vol. 4, No. 1 (1946), pp. 9 - 19.

Karman, T. von and Tsien, H. "Buckling of Thin Cylindrical Shells in Axial Compression". Journal of the Aeronautical Sciences, Vol.8, No. 8 (1941) pp. 203-213.

Karman, T. von and Tsien, H. "The Buckling of Spherical Shells by External Pressure". Journal of the Aeronautical Sciences, Vol.7, No.2, (1939) pp. 43-50

C. Pamphlets.

Plywood Manufacturers Association of British Columbia, Douglas Fir Plywood Technical Handbook, Vancouver. Keystone Press.

Plywood Manufacturers Association of British Columbia, Douglas Fir Plywood for Concrete Form Work. Vancouver Keystone Press.